increased risk for CHD development than female hypercholesterolemic patients. However, our result clearly revealed that for the patients with both hypercholesterolemia and type 2 diabetes, the gender difference in the risk for coronary events becomes smaller (3.33, $p < 0.001$–1.94, $p = 0.057$). The patients' baseline characteristics, such as hypertension ($p = 0.017$ with type 2 diabetes and $p < 0.001$ without type 2 diabetes), electrocardiogram abnormality ($p = 0.024$ and 0.009, respectively), family history of CHD ($p = 0.170$ and $p < 0.001$, respectively) and smoking habit ($p = 0.200$ and 0.006, respectively) increase the risk for coronary events as expected.

On the other hand, our analysis showed that alcohol consumption had tendency to reduce the risk of coronary events for hypercholesterolemic patients with or without type 2 diabetes, although it was not statistically significant ($p = 0.072$ and 0.105, respectively). However, it should be noted that the subjects who consumed alcohol in the current study were *light-moderate* drinkers, (approximate average was 38 g ethanol/day), thus this influence of alcohol consumption on the coronary events might be limited to that level and may differ from heavy drinkers without diabetes.

Also, obesity did not appear to be a risk factor of coronary events for both hypercholesterolemic patients with and without type 2 diabetes in this analysis ($p = 0.187$ and 0.510, respectively). (The reason of this result is explained in Section 3.).

The risk of coronary event for oral hypoglycemic agents 1.78 (95% CI 1.04–3.03, $p = 0.036$), insulin 5.35 (95% CI 2.65–10.81, $p < 0.001$).

In this study, 1136 hypercholesterolemic patients had slightly high fasting blood glucose level (6.11–6.99 mmol/l), and 11 of these subjects developed coronary events in the study period. We calculated the relative risk of developing a coronary events for the hypercholesterolemic subjects with slightly high fasting blood glucose level compared to those with hypercholesterolemia alone (adjusted with age, sex, hypertension and smoking). The relative risks was 2.11 (95% CI 1.14–3.91, $p = 0.017$).

3. Discussions

The J-LIT, a long-term prospective cohort study on the use of simvastatin, is the first epidemiological study in Japan to demonstrate the relationship between serum lipid levels and the incidence of CHD in Japanese patients with hypercholesterolemia [17]. The J-LIT study provides excellent data to elucidate the coronary event risk associated with having both hypercholesterolemia and type 2 diabetes.

Since the J-LIT study was conducted in a standard clinical environment in a target population of hypercholesterolemic patients throughout the country, the findings could be reasonably extrapolated to the general Japanese population. The study monitored hypercholesterolemic patients treated with low-dose simvastatin (5–10 mg/day) over 6 years. Of the 41,801 subjects, 6554 patients (15.7%) had type 2 diabetes as well. This morbidity was lower than that of the US study which reported 25% of hypercholesterolemic study patients had type 2 diabetes [18]. The traditional Japanese diet, constituted mainly of vegetables, carbohydrate and low protein, may contribute to the lower morbidity of type 2 diabetes, although the younger generations' diet has become steadily westernized.

We have already reported that serum TC and LDL-C levels were positively correlated and serum HDL-C level was inversely correlated with the risk of CHD in the hypercholesterolemic patients without a history of CHD in the J-LIT study [7]. In the present investigation, the same pattern of risk for coronary events can be seen in both hypercholesterolemic patients with and without type 2 diabetes. For the patients with type 2 diabetes, the relative risk was higher (2.06, 95% CI 1.06–4.02, $p = 0.033$) in 2.82 mmol/l for TG. We further analyzed the adjusted relative risks for LDL-C or HDL-C. After that, the risks for TG adjusted with LDL-C did not change, while the risk for TG disappeared (1.33, 95% CI 0.66–2.68, $p = 0.432$) after the adjustment with HDL-C. We observed that HDL-C was confounding factor for the risk of TG for coronary events.

This study demonstrated that hypercholesterolemic patients with slightly high fasting blood glucose level have the same level of increased risk for coronary events as hypercholesterolemic subjects with typical type 2 diabetes. Although the fasting blood glucose level was not matched high to the diabetes mellitus, such patients should be managed as strictly as the same as the patients with type 2 diabetes and hypercholesterolemia. Early management for glucose control, including diet and exercise are necessary when the fasting blood glucose level were between 6.11 and 6.99 mmol/l in order to prevent later serious outcomes.

We also found that alcohol intake at low to moderate levels may reduce the risk of coronary events in patients with hypercholesterolemia, with and without type 2 diabetes. In Japan, for patients with lifestyle-associated diseases, such as hyperlipidemia and type 2 diabetes, alcohol intake has been thought to accelerate the progression of CHD. Thus alcohol consumption is sometimes even prohibited by the physicians in these patients. However, based on this large scale J-LIT study results, further consideration should be given to the role of alcohol consumption at different levels.

Obesity has been considered as a risk factor of type 2 diabetes and CHD. In this study, obesity was not shown as a risk factor. The standard diagnosis criteria for the metabolic syndrome revised lately, adopts the waist circumference for defining obesity (male: >85 cm, female: >90 cm). It was not observed that obesity was an independent risk factor in the present study. It might be caused by that BMI instead of waist circumference was utilized in this. This report based on the J-LIT study, for the first time, clearly reveals that the Japanese hypercholesterolemic patients with type 2 dia-

betes have higher risk for developing coronary events. Thus, Japanese patients with both risk factors need more careful and strict management of LDL-C, HDL-C and TG in addition to the blood glucose control for the prevention of coronary events.

4. Limitation

This study is post hoc non-randomized, observational subanalysis.

Acknowledgment

This study is in part supported by a grant from the Banyu Pharmaceutical Co., Ltd., Tokyo, Japan.

References

[1] National Cholesterol Education Program. Second report of the expert panel on detection, evaluation, and treatment of high blood cholesterol in adults (Adult treatment panel II). Circulation 1994;89:1333–445.
[2] Castelli WP, Garrison RJ, Wilson PW, et al. Incidence of coronary heart disease and lipoprotein cholesterol levels. The Framingham Study. JAMA 1986;256:2835–8.
[3] Stamler J, Wentworth D, Neaton JD. Is the relationship between serum cholesterol and risk of premature death from coronary heart disease continuous and graded? Findings in 356,222 primary screenees of the Multiple Risk Factor Intervention Trial (MRFIT). JAMA 1986;256:2823–8.
[4] Keys A, Menotti A, Aravanis C, et al. The Seven Countries Study 2,289 deaths in 15 years. Prev Med 1984;2:141–54.
[5] Pedersen TR, et al. Randomized trial of cholesterol lowering in 4444 patients with coronary heart disease: the Scandinavian Simvastatin Survival Study (4S). Lancet 1994;344:1383–9.
[6] Sacks FM, Pfeffer MA, Moye LA, et al. The effect of pravastatin on coronary events after myocardial infarction in patients with average cholesterol levels. N Engl J Med 1996;335:1001–9.
[7] Matsuzaki M, et al. A large scale cohort study on the relationship between serum cholesterol levels and coronary events in Japanese patients with hypercholesterolemia: Japan Lipid Intervention Trial (J-LIT)—primary prevention study. Circ J 2002;66:1087–95.
[8] Horiuchi H, et al. Primary cardiovascular events and serum lipid levels in elderly Japanese with hypercholesterolemia under 6-year simvastatin treatment: a sub-analysis of the J-LIT Study. J Am Geriatr Soc 2004;52:1981–7.
[9] Kodama K, Sasaki H, Shimizu Y. Trend of coronary heart disease and its relationship to risk factors in a Japanese population: a 26-year follow-up. Hiroshima/Nagasaki study. Jpn Circ J 1990;54:414–21.
[10] Wakugami K, Iseki K, Kimura Y, et al. Relationship between serum cholesterol and the risk of acute myocardial infarction in a screened cohort in Okinawa, Japan. Jpn Circ J 1998;62:7–14.
[11] Okayama A, Ueshima H, Marmot MG, et al. Changes in total serum cholesterol and other risk factors for cardiovascular disease in Japan 1980–1989. Int J Epidemiol 1993;22:1038–47.
[12] Investigating Committee on Guidelines for Diagnosis Treatment of Hyperlipidemias Japan, Atherosclerosis Society. Guidelines for diagnosis and treatment of hyperlipidemias in adults. Jpn J Atheroscler 1997;25:1–34.
[13] Kawamori R. Diabetes trends in Japan. Diabetes Metab Res Rev 2002;18:S9–S13.
[14] Gotto AM. Lipid management in diabetic patients: lessons from prevention trials. Am J Med 2002;112(Suppl 8A):19S–26S.
[15] Matsuzawa Y, Itakura H, Kita T, et al. Design and baseline characteristics of a cohort study in Japanese patients with hypercholesterolemia: The Japan Lipid Intervention Trial (J-LIT). Curr Therapeu Res 2000;61:219–43.
[16] Cox DR. Regression models and life tables (with discussion). J R Stat Soc 1972;B34:187–220.
[17] Matsuzawa Y, et al. Sustained reduction of serum cholesterol in low-dose 6-year simvastatin treatment with minimum side effects in 51,321 Japanese hypercholesterolemic patients: implication of the J-LIT study, a large scale nationwide cohort study. Circ J 2003;67:287–94.
[18] Rubins HB, et al. Gemfibrozil for the secondary prevention of coronary heart disease in men with low levels of high density lipoprotein cholesterol. N Engl J Med 1999;341:410–8.

Available online at www.sciencedirect.com
ScienceDirect
Biochemical and Biophysical Research Communications 351 (2006) 865–871
BBRC
www.elsevier.com/locate/ybbrc

Protection of atherogenesis in thromboxane A2 receptor-deficient mice is not associated with thromboxane A2 receptor in bone marrow-derived cells

Xin Zhuge [a,1], Hidenori Arai [b,*], Yang Xu [a], Toshinori Murayama [a], Takuya Kobayashi [d], Shuh Narumiya [d], Toru Kita [c], Masayuki Yokode [a]

[a] *Department of Clinical Innovative Medicine, Kyoto University Graduate School of Medicine, 54 Kawahara-cho, Shogoin, Sakyo-ku, Kyoto 606-8507, Japan*
[b] *Department of Geriatric Medicine, Kyoto University Graduate School of Medicine, 54 Kawahara-cho, Shogoin, Sakyo-ku, Kyoto 606-8507, Japan*
[c] *Department of Cardiovascular Medicine, Kyoto University Graduate School of Medicine, 54 Kawahara-cho, Shogoin, Sakyo-ku, Kyoto 606-8507, Japan*
[d] *Department of Cell Biology, Kyoto University Graduate School of Medicine, 54 Kawahara-cho, Shogoin, Sakyo-ku, Kyoto 606-8507, Japan*

Received 6 October 2006
Available online 2 November 2006

Abstract

In the previous study, we generated mice lacking thromboxane A2 receptor (TP) and apolipoprotein E, apoE$^{-/-}$TP$^{-/-}$ mice, and reported that the double knockout mice developed markedly smaller atherosclerotic lesions than those in apoE$^{-/-}$ mice. To investigate the mechanism responsible for reduced atherosclerosis in apoE$^{-/-}$TP$^{-/-}$ mice, we examined the role of TP in bone marrow (BM)-derived cells in the development of the atherosclerotic lesions. When we compared the function of macrophages in apoE$^{-/-}$ and in apoE$^{-/-}$TP$^{-/-}$ mouse *in vitro*, there was no difference in the expression levels of cytokines and chemokines after stimulation with lipopolysaccharide. We then transplanted the BM from either apoE$^{-/-}$ or apoE$^{-/-}$TP$^{-/-}$ mice to either apoE$^{-/-}$ or apoE$^{-/-}$TP$^{-/-}$ mice after sublethal irradiation. After 12 weeks with high fat diet, we analyzed the atherosclerotic lesion of aortic sinus. When the BM from apoE$^{-/-}$ or apoE$^{-/-}$TP$^{-/-}$ mice was transplanted to apoE$^{-/-}$ mice, the lesion size was almost the same as that of apoE$^{-/-}$ mice without BM transplantation. In contrast, when the BM from apoE$^{-/-}$ or apoE$^{-/-}$TP$^{-/-}$ mice was transplanted to apoE$^{-/-}$TP$^{-/-}$ mice, the lesion size was markedly reduced. These results indicate that the protection of atherogenesis in TP$^{-/-}$ mice is not associated with TP in BM-derived cells.

Keywords: Thromboxane A2 receptor; Macrophage; Atherosclerosis; Apolipoprotein E-deficient mice

The lipid mediator thromboxane A2 (TXA2) is a biologically active metabolite of arachidonic acid, which is synthesized from prostaglandin endoperoxide [1] via thromboxane synthase [2]. In addition to its major role as a powerful platelet aggregator [3], TXA2 can induce potent vasoconstriction, stimulate the proliferation of vascular smooth muscle cells [4], and is a positive inotropic agent of the heart [5]. Accumulating evidence indicates that increased production of TXA2 is associated with vascular pathology, particularly with atherosclerosis of coronary artery disease and accelerated atherosclerosis of saphenous vein graft [6,7]. The efficacy of low-dose aspirin in the secondary prevention of cardiovascular events is also attributed to inhibition of TXA2 production by platelets [8].

The biological action of TXA2 is mediated via its specific membrane TXA2 receptor (TP). TP has been shown to play an important role in the development of atherosclerosis in the apolipoprotein E-deficient (apoE$^{-/-}$) mouse [9], in which they demonstrated that blockade of TP inhibits atherosclerosis by a mechanism independent of platelet-derived TXA2. Moreover, the response to injury-induced

* Corresponding author. Fax: +81 75 751 3463.
E-mail address: harai@kuhp.kyoto-u.ac.jp (H. Arai).
[1] Present address: Department of Official Ward, Tianjin Medical University Hospital, Tianjin, China.

0006-291X/$ - see front matter © 2006 Elsevier Inc. All rights reserved.
doi:10.1016/j.bbrc.2006.10.121

vascular proliferation is markedly exaggerated in transgenic mice with vascular overexpression of the human TP gene, and this response is reduced by TP antagonist [10].

Human TP is a G protein-coupled receptor composed of 343 amino acids [1,11]. mRNA for TP is expressed in a large number of tissues such as lung, kidney, brain, and thymus, and in various cell types such as smooth muscle cells, endothelial cells, epithelial cells, and in platelets [12]. Recent study showed that TP expression is significantly increased in human atherosclerotic coronary arteries compared with normal vessels [13]. Cell culture studies also indicate that TP may be related to the development of atherosclerosis by a mechanism by which TXA2 binds to TP located on the endothelial cell surface and augments the expression of endothelial adhesion molecules [14–16]. Other studies show that stimulation of TP in human umbilical vein endothelial cells may result in an increase in the activity of monocytes and T cells through monocyte chemoattractant protein-1 (MCP-1) [17], and TXA2 affects the proliferation of vascular smooth muscle cells [18].

The pathophysiological role of monocytes and macrophages in atherogenesis is well documented [19]. The accumulation of LDL cholesterol in bone marrow (BM)-derived macrophages in the artery wall and their consequent conversion into foam cells is an early step in atherogenesis [20]. Macrophages contain TX synthase and release large amounts of TXA2, when transformed into foam cells with modified LDL [21]. In our previous study, we found the protective effect of TP deficiency on the development of atherosclerosis by generating apoE$^{-/-}$ TP$^{-/-}$ mice, in which we showed significant suppression in the lesion areas of proximal aorta by 70% compared with those of apoE$^{-/-}$ mice [22]. Recently, Egan et al. confirmed the efficacy of the TP antagonist in retarding murine atherosclerosis. Further, the immunostaining with anti-laminin and anti-α-actin antibodies of the aortic lesion area showed that the inhibition of TP resulted in morphological changes in plaque by a decrease in macrophages and apoptotic cells in the subendothelium areas and an increase in SMCs in fibrotic caps, which made the plaque into a more stable phenotype [40]. It is suggested that BM-derived precursors can give rise to vascular cells that contribute to the repair, remodeling, and lesion formation of the arterial wall under certain circumstances [23].

The present study was, therefore, designed to elucidate the mechanism responsible for the prevention of advanced atherosclerosis in apoE$^{-/-}$TP$^{-/-}$ mice. Specifically, utilizing bone marrow (BM) transplantation technique, we tried to address how important TP in BM-derived monocyte-macrophages is in this process.

Methods

Animal study. All experimental protocols were performed in accordance with the guidelines of Kyoto University, Japan. ApoE$^{-/-}$ mice (hybrid: C57BL/6 × 129ola) were a generous gift from Dr. Edward M. Rubin in University of California at Berkeley [24]. These mice were mated with C57BL/6 mice to produce F_1 hybrids. The F_1 apoE$^{+/-}$ mice were then backcrossed to C57BL/6 at least five times. ApoE$^{-/-}$ mice on a C57BL/6 background were subsequently generated. TP$^{-/-}$ mice with C57BL/6 background were generated as previously described [25] The mice were kept in a temperature-controlled facility on a 14-h light/10-h dark cycle, with free access to food and water. Mice were fed a normal chow diet containing 8.7% (wt/wt) fat and 0.063% (wt/wt) cholesterol (Oriental Yeast, Chiba, Japan) for the experiment except BM transplantation (BMT).

Culture of macrophage. Peritoneal macrophages were harvested as described [26] from wild-type (WT) C57BL/6, TP$^{-/-}$, apoE$^{-/-}$, and apoE$^{-/-}$TP$^{-/-}$ double knockout mice. Cells (3×10^6/ml) were grown in Dulbecco's modified Eagle's medium (DMEM) supplemented with 10% fetal calf serum, 50 U/ml penicillin, and 50 μg/ml streptomycin in 150 cm^2 or 6-well tissue culture plates and maintained at 37 °C in 5% CO_2 and 95% air. Before pretreatment or stimulation, cells were incubated in serum-free media for 18 h.

RT-PCR. Total RNA was isolated using TRIzol Reagent (Invitrogen, Carlsbad, CA). One to 1.5 μg of total RNA was primed with oligo(d)T for first strand cDNA synthesis in a 20 μl reaction using SuperScript™ II Reverse Transcriptase, according to the manufacturer's instructions (Invitrogen). The transcript cDNA was amplified with TP-specific set of primers 5′-AAGCTTGGGTTTCAGGGACCTG-3′ (forward) and 5′-ACTTTGTTGCAGACACCACCTGTC-3′ (reverse) [22] by 35 cycles PCR by denaturation at 94 °C for 1 min, annealing at 65 °C for 1 min, and extension at 72 °C for 80 s in DNA Engine Peltier Thermal Cycler PTC-200 (MJ Research, Waltham, MA). Amplified products were visualized in a 1% agarose gel containing 0.1 μg/ml of ethidium bromide.

p44/42 MAP kinase assay. Before stimulation, cells were incubated in serum-free media overnight to minimize basal p44/42 MAP kinase activity. Cells were then stimulated with I-BOP (Cayman Chemical, Ann Arbor, MI), a potent TP agonist, for 5 min. p44/42 MAP kinase activation was measured following the directions provided by p44/42 MAP Kinase Assay Kit (Cell Signaling Technology, Beverly, MA). Briefly, the cell lysate was collected by ice-cold cell lysis buffer provided by the kit. Immunoprecipitation was done by using immobilized phospho-p44/42 MAP kinase (Thr202/Tyr204) monoclonal antibody. Subsequently, protein from each sample was loaded onto a sodium dodecyl sulfate 12% polyacrylamide gel, subjected to electrophoresis, and transferred onto a PVDF membrane. For immunodetection, the membrane was blocked in a 5% powered-milk solution in TBS-T (20 mM Tris, 500 mM NaCl, and 0.05% Tween 20, pH 7.4) for 30 min, and incubated overnight with rabbit anti-phospho-ELK-1 antibody (1:1000) at 4 °C. After being washed with TBS-T for three times, the membrane was incubated with HRP-conjugated anti-rabbit secondary antibody (1:2000) for 1 h, and was incubated with detection reagents.

TXB2 assay. Enzyme immunoassay for TXB2 was performed by TXB2 immunoassay kit (Cayman Chemical) according to manufacturer's instructions. Bio-Rad DC Protein Assay (Bio-Rad Laboratories, Hercules, CA) was used to measure the protein concentration of the cells.

BMT. Donor apoE$^{-/-}$ or apoE$^{-/-}$TP$^{-/-}$ mice, 8–10 weeks old, were sacrificed, and their BM cells were harvested from the femurs as described [27–29]. Recipient apoE$^{-/-}$ or apoE$^{-/-}$TP$^{-/-}$ male mice, 7 weeks old, were irradiated with 9 Gy of γ ray in a single dose using the Gammacell 40 Exactor Irradiator (Nordion International). Four hours later, $3–5 \times 10^6$ BM cells in 0.5 ml PBS were transplanted by tail-vein injection as described [28]. After BMT, the mice were placed on a high fat diet containing 20% fat and 0.3% cholesterol (Oriental Yeast, Chiba, Japan) to accelerate the development of atherosclerosis. BM reconstitution was quantified by real-time PCR of genomic DNA as described below.

Quantification of TP DNA by real-time PCR. Genome DNA was prepared from whole blood cells from donor and recipient mice before and 2 weeks after BMT following the directions provided by QIAampDNA Blood Mini Kit (Qiagen, Valencia, CA). The relative quantities of TP were measured by a real-time PCR using a commercially available kit (TaqMan Universal PCR Master Mix, Applied Biosystems, Foster City, CA) with 18S rRNA as an endogenous control. The primer sequences for TP were as follows: 5′-ATCGTGGCGTCGCAACA-3′ (forward) and 5′-ACCATAG CTACCCCCATGAAGTAG-3′ (reverse). The TaqMan probe sequence for TP was 5′-FAM-CTGCCTTGTTGGACTGGCGAGCC-TAMAR-3′.

Thermal cycling conditions for TP consisted of an initial 95 °C for 10 min, followed by 40 cycles of 15 s at 95 °C and 1 min at 60 °C. Cycle threshold (C_T) was determined according to the instructions from Applied Biosystems. The data were analyzed by the comparative C_T method and were confirmed by the standard curve method, as described [30].

RNase protection assay. Mouse macrophages were harvested and incubated in serum-free media for 18 h, followed by exposure to vehicle or lipopolysaccharide (LPS, 1.0 μg/ml) for 2 h. Total RNA was obtained by TRIzol extraction. mRNA expressions for tumor necrosis factor (TNF), interleukin (IL)-1α and -1β, macrophage inflammatory protein (MIP)-2, and monocyte chemoattractant protein (MCP)-1 were determined by RNase protection assay. Briefly, ^{32}P-labeled anti-sense RNA probes were generated from custom RiboQuant™ Multi-Probe Template sets (PharMingen, San Diego, CA) and hybridized with target RNA according to the manufacturer's recommendations. The RNase-protected probe was then purified and resolved on denaturing polyacrylamide gels. The gels were developed subsequently on a film, and expressed mRNA was identified by bands corresponding to the expected fragment size.

Tissue preparation and quantification of atherosclerotic lesion. After feeding with high fat diet for 12 weeks, mouse tissue was prepared as described [31–33]. Briefly, each mouse was sacrificed and the freshly removed heart was snap-frozen in O.C.T Compound (Sakura Finetek USA Inc., Torrance, CA) and sequentially cut into 6-μm-thick sections around the aortic sinus, followed by oil red-O-staining (Sigma Chemical, St. Louis, MO) and nuclear counterstaining (Mayer's hematoxylin solution, Wako Pure Chemical Industries, Osaka, Japan). Quantitative analysis was evaluated by Image-Pro Plus (Media Cybernetics, Silver Spring, MD) to measure the surface area of the lesion and total surface area of the tissue. The fraction area of the lesion was calculated as dividing surface of the lesion by the surface of the vessel [34]. For each animal, 25 sequential sections were examined and the mean of fraction area of the lesion was calculated and expressed as percent.

Bleeding time. Bleeding time was assessed according to a previously reported method [35]. In brief, mice were placed in a holder, and their tails were transected 1 cm proximal from the tip. The remaining tail was immersed immediately into PBS maintained at 37 °C, and the time until visible bleeding stops was measured. The hemostasis was conducted by electric burn in case of losing too much blood when bleeding time >10 min.

Serum cholesterol measurement. Mice were fasted for 4 h in the morning before blood was drawn at the time points before BMT, and 8 and 12 weeks after BMT. The samples were centrifuged to isolate serum and total cholesterol level was determined with a commercially available enzymatic reaction kit (Toyobo, Osaka, Japan) according to the manufacturer's instructions.

Statistical analysis. Data are expressed as means ± SD and were analyzed by ANOVA using StatView software (version 5.0, SAS, Cary, NC). $P < 0.05$ was considered statistically significant.

Results

TP expression in mice macrophage

We first examined the expression of TP in mouse macrophages by RT-PCR (Fig. 1a). TP expression was found in macrophages both from WT and apoE$^{-/-}$ mice, while no expression was found in TP$^{-/-}$ mice as expected.

I-BOP stimulated P44/42 MAP kinase phosphorylation

To show that the TP function of macrophages in TP$^{-/-}$ mice is absent, we have determined the p44/42 MAP kinase activity after stimulation with TP agonist, I-BOP. *In vitro* kinase assay was used to determine the activation of p44/42 MAP kinase. Peritoneal macrophages from WT and TP$^{-/-}$ mice were stimulated with I-BOP (100 nM) for 0 or 5 min. In WT cells I-BOP induced the activation of p44/42 MAP kinase at 5 min, while no p44/42 MAP kinase activation was found in TP$^{-/-}$ cells (Fig. 1b).

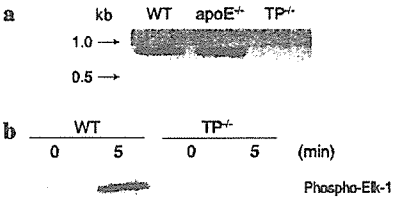

Fig. 1. TP expression and activation of p44/42 MAP kinase in mouse macrophages. Total RNA was extracted from peritoneal macrophages of WT, apoE$^{-/-}$, and TP$^{-/-}$ mice, and then RT-PCR was performed for TP expression (a). After macrophages (3×10^6/ml) from WT and TP$^{-/-}$ mice were incubated with serum-free DMEM for 18 h, they were stimulated with I-BOP (100 nM) for 5 min, and the cell lysate was collected for immunoblot analysis using anti-p44/42 MAP kinase antibody (b).

TXB2 synthesis by macrophages

To examine whether TXA2 can be induced by inflammatory stimuli in macrophages, we stimulated the cells from WT, TP$^{-/-}$, apoE$^{-/-}$, and apoE$^{-/-}$TP$^{-/-}$ mice with LPS and examined the TXB2 synthesis. As shown in Fig. 2, LPS (10 μg/ml) caused about three times of TXB2 production as compared with the basal level in each cell type. However, induction of macrophage TXB2 production after LPS stimulation did not differ among the four mouse groups irrespective of the presence of TP allele.

LPS-induced production of proinflammatory cytokines and chemokines

We next examined the production of proinflammatory cytokines and chemokines from macrophages by RNase protection assays with specific probes *in vitro*. Peritoneal

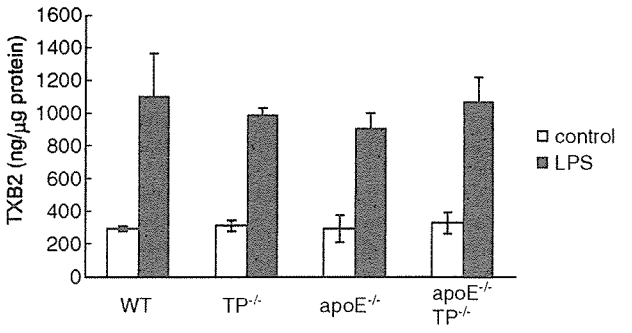

Fig. 2. LPS-stimulated TXB2 production in macrophage. After macrophages (3×10^6/ml) were serum-starved for 18 h, they were stimulated with LPS (10 μg/ml) for 24 h. Supernatants were collected and measured for TXB2 production. Cell lysate was collected for the determination of protein contents. Data are means ± SD from four independent experiments.

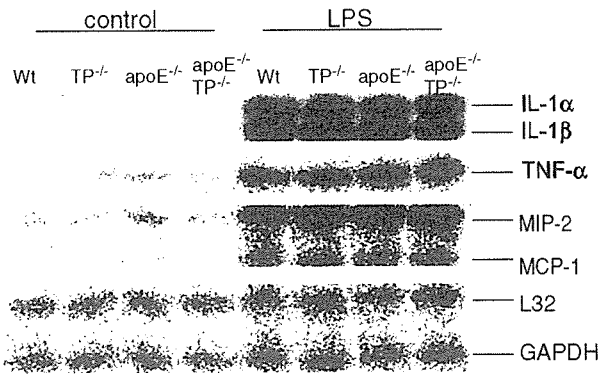

Fig. 3. Chemoattractant and inflammatory cytokine expression in peritoneal macrophages. Macrophages harvested from WT, $TP^{-/-}$, $apoE^{-/-}$, and $TP^{-/-}apoE^{-/-}$ mice were stimulated with or without LPS (1 μg/ml) for 2 h. Total RNA was then extracted from the cells and the RNase protection assay was performed for TNF-α, IL-1α, IL-1β, MCP-1, MIP-2, L32, and GAPDH.

macrophages were harvested from WT, $TP^{-/-}$, $apoE^{-/-}$, and $apoE^{-/-}TP^{-/-}$ mice, and were exposed to vehicle or LPS (1.0 μg/ml) for 2 h. Total RNA was then extracted to perform RNase protection assay. We found no significant difference in the expression levels of inflammatory cytokines such as TNF-α and IL-1α, 1β or chemokines such as MIP-2 and MCP-1 either in a resting state or after stimulation with LPS in all kinds of cells (Fig. 3).

BMT study

To determine the contribution of TP in monocyte/macrophage and platelets in atherogenesis, we conducted BMT experiments as follows: BMT from $apoE^{-/-}TP^{-/-}$ mice to $apoE^{-/-}$ mice (group 2, $n = 5$) or from $apoE^{-/-}$ to $apoE^{-/-}TP^{-/-}$ mice (group 4, $n = 4$) as described in Methods. As each control, the BM cells from $apoE^{-/-}$ mice were transplanted to $apoE^{-/-}$ mice (group 1, $n = 5$) or from $apoE^{-/-}TP^{-/-}$ to $apoE^{-/-}TP^{-/-}$ mice (group 3, $n = 4$). The transplanted mice were fed with high fat diet. To examine what percentage of the blood cells is derived from the donor BM, blood cells from the recipient mice were harvested before and 2 weeks after BMT, and TP expression in whole blood cells was studied by quantitative real-time-PCR. When the BM of $apoE^{-/-}TP^{-/-}$ was transplanted to $apoE^{-/-}$ mice, the recipients showed as low as 10% ($n = 4$) of TP expression as compared with that before BMT. In contrast, when the BM of $apoE^{-/-}$ was transplanted to $apoE^{-/-}TP^{-/-}$ mice, more than 90% of the blood cells were positive for TP, indicating successful reconstitution of BM in the recipient mice with the donor cells. We also confirmed the BM reconstitution by measuring the bleeding time. As expected, the bleeding time of $apoE^{-/-}$ mice transplanted with the BM of $apoE^{-/-}TP^{-/-}$ mice was prolonged and almost the same as that of $apoE^{-/-}TP^{-/-}$ mice. The bleeding time of each group (1–4) of mice was 155 ± 16, 566 ± 33, 490 ± 70, and 123 ± 18 s, respectively, indicating

Table 1
Total cholesterol levels of 4 groups of mice before and after BMT

Donor	Recipient	Baseline	After 8 weeks	After 12 weeks
$apoE^{-/-}$	$apoE^{-/-}$	384 ± 24	999 ± 131	863 ± 147
$apoE^{-/-}TP^{-/-}$	$apoE^{-/-}$	359 ± 27	847 ± 77	774 ± 93
$apoE^{-/-}TP^{-/-}$	$apoE^{-/-}TP^{-/-}$	375 ± 35	1033 ± 131	971 ± 142
$apoE^{-/-}$	$apoE^{-/-}TP^{-/-}$	442 ± 43	802 ± 132	802 ± 114

Values are expressed as means ± SD (mg/dL).

that TP in platelets is absent in mice transplanted with the BM of $apoE^{-/-}TP^{-/-}$ mice. After 4 weeks of BMT, the plasma white blood cell (WBC) and platelet counts were similar before and after sublethal irradiation and BMT (data not shown).

We measured the serum total cholesterol levels at time points before BMT, and 8 and 12 weeks after BMT. There were no significant differences among the four groups (1–4) in all time points that we observed by ANOVA (Table 1). The mice were sacrificed and the aortic sinus was analyzed by oil red-O staining (Fig. 4a). As shown in Fig. 4a, we found no significant difference in the fraction area of the atherosclerotic lesion either between group 1 and 2 or between group 3 and 4. The fraction area of the lesion in recipient $apoE^{-/-}TP^{-/-}$ mice (groups 3 and 4) was significantly smaller than that in recipient $apoE^{-/-}$ mice (groups 1 and 2) after BMT, irrespective of the donor BM origin (Fig. 4b). The fraction area of the lesion in recipient $apoE^{-/-}$ mice was almost the same as that of $apoE^{-/-}$ mice, which were not subjected to BMT (data not shown).

Discussion

In this study, we have shown that TP expressed in BM-derived cells such as monocyte/macrophage and platelets does not play a major role in the development of atherosclerosis in $apoE^{-/-}$ mice. This is an unexpected finding, because the major cells accumulated in atherosclerotic lesions are macrophages in $apoE^{-/-}$ mice, and more recently it is reported that macrophages were decreased in the atherosclerotic lesions by TP antagonist in $apoE^{-/-}$ mice [40]. Our study also indicates that TP expressed in platelets does not play an essential role in atherogenesis in $apoE^{-/-}$ mice, either.

BMT studies in gene-targeted mice have been a powerful tool to examine the contribution of various genes expressed by macrophages to foam-cell formation and atherogenesis. Recently, Babaev et al. [41] examined the impact of COX-1 expression by BM-derived cells on early atherosclerotic lesion formation in $apoE^{-/-}$ and $LDLR^{-/-}$ mice and found that both of the recipient mice reconstituted with $COX\text{-}1^{-/-}$ BM cells increased atherosclerotic lesions. In their study, COX-1 deficiency in BM-derived cells does not suppress early atherosclerosis in $apoE^{-/-}$ and $LDLR^{-/-}$ mice despite elimination of platelet TX production. In this study, we first generated TP-deficient condition

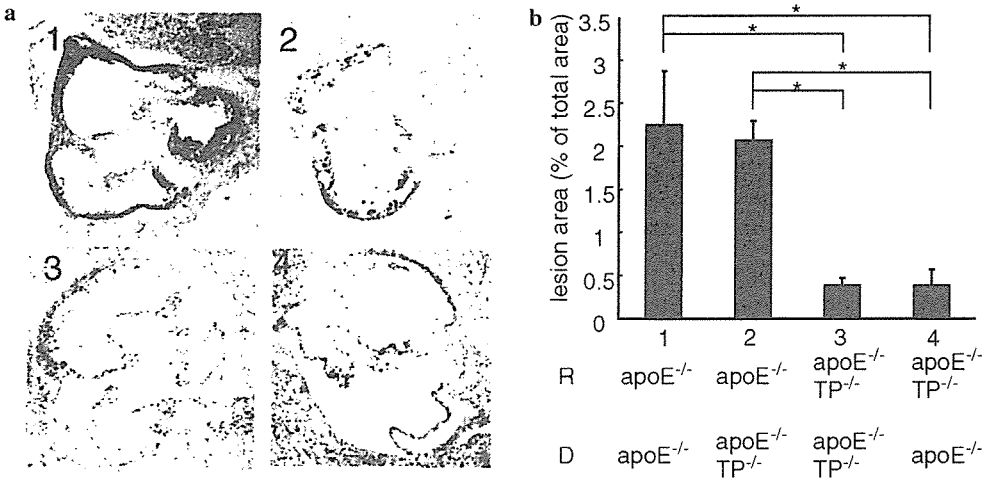

Fig. 4. Atherosclerotic lesion in BMT mice. (a) Oil red-O and hematoxylin staining was performed for aortic roots (objective 4). The representative section from apoE$^{-/-}$ mice transplanted with BM cells from apoE$^{-/-}$ (1) or apoE$^{-/-}$TP$^{-/-}$ mice (2). The representative section from apoE$^{-/-}$TP$^{-/-}$ mice transplanted with BM cells from apoE$^{-/-}$TP$^{-/-}$ (3) or apoE$^{-/-}$ mice (4). (b) Quantification of atherosclerotic lesion areas in each group of mice fed with the high fat diet for 12 weeks after BMT. Sections were stained and the fraction area of the lesion was measured for the atherosclerotic lesions. Data are represented as means ± SD from 25 sections in each group. $^{*}p < 0.01$; R, recipient; D, donor.

in blood cells in apoE$^{-/-}$ mice by BMT to examine the role of TP in BM-derived cells. Our results indicate that the phenotype of atherosclerotic lesions is dependent on the recipient, not on the donor and that the BM-derived cells in apoE$^{-/-}$TP$^{-/-}$ mice do not play an essential role in lesion formation. Thus the function of TP in blood cells is not sufficient to explain this protective effect in TP$^{-/-}$ mice. Because there is no antibody available for mouse TP for immunostain, in situ hybridization of TP in atherosclerosis plaque together with counterstaining by cell-specific antibodies may be an alternative approach in the future to identify the major cell source of TP in atherogenesis.

Inhibitors of TXA2 synthase and TP antagonists improve pathophysiological events associated with atherosclerosis [9,10]. TP is a G protein-coupled receptor, which is linked to phospholipase C activation leading to an increase in cytosolic free calcium [36]. Here we first confirmed that TP is expressed in mouse macrophages and discovered that TP agonists induced MAP kinase activation in those cells, but not in TP$^{-/-}$ macrophages. This raises the possibility that TP can be involved in biological responses of macrophage relevant to the pathogenesis of atherosclerosis. Since TXA2 is produced locally by many cells including monocytes or macrophages [37–39], we first examined whether TP-deficiency in macrophage can affect the TXA2 synthesis *in vitro*. LPS stimulated TXB2 secretion, a stable metabolite of TXA2, by WT macrophages in a dose- and time- dependent manner (data not shown). However, we could not find decreased TXB2 production in TP-deficient macrophages (Fig. 2), or in urinary 2,3-din-or TBX2 levels of TP-deficient mice (data not shown). These data indicate that the anti-atherosclerotic effect may not be attributed to the low TXA2 synthesis in apoE$^{-/-}$TP$^{-/-}$ mice.

Next, we examined the function of TP-deficient macrophage by RNase protection assay for pertinent cytokines and chemokines, which play critical roles in vascular inflammation. However, the mRNA levels for TNF-α, IL-1α and -1β, MIP-2, and MCP-1 were not significantly different between TP$^{-/-}$ macrophages and TP$^{+/+}$ ones both in a resting state and in a condition stimulated with LPS. Thus macrophages function normally, even if they lack TP expression.

Taken together, TP in monocyte-macrophage lineage does not play, at least, a central regulatory role in atherogenesis in apoE$^{-/-}$ mice. Indeed, in the previous study, we have found that ICAM-1 expression on endothelial cells (ECs) overlying the plaques of apoE$^{-/-}$TP$^{-/-}$ mice was significantly lower, suggesting that TP deficiency can affect the interaction of ECs with platelets or leukocytes [22]. Ashton et al. indicated that TXA2 mimetic is a potent antagonist for VEGF-induced EC migration and differentiation [42]. It was also reported that the TP antagonist improved endothelium-dependent vasodilation [43]. Therefore, TP expressed in cells other than macrophages and platelets might contribute to this protective effect. Endothelial specific TP-knockout mice would be a promising approach to address this issue and should be done in the future.

Acknowledgments

This study was supported by Grants-in-Aid from the Ministry of Education, Science, Sports, and Culture of Japan (20045982, 12671111, 14571093, and 13307034); Center of Excellence grants from the Ministry of Education, Science, Sports, and Culture of Japan (12CE2006); a research grant for health sciences from the Japanese Ministry of Health and Welfare; Establishment of International

COE for Integration of Transplantation Therapy and Regenerative Medicine (COE program of the Ministry of Education, Culture, Sports, Science and technology, Japan). We thank Akiko Kato for her excellent technical assistance. X.Z. was supported by 21st century Center of Excellent program from the Ministry of Education, Culture, Sports, Science and Technology, Japan.

References

[1] S. Narumiya, Y. Sugimoto, F. Ushikubi, Prostanoid receptors: structures, properties, and functions, Physiol. Rev. 79 (1999) 1193–1226.
[2] J.B. Smith, Pharmacology of thromboxane synthetase inhibitors, Fed. Proc. 46 (1987) 139–143.
[3] P.V. Halushka, D.E. Mais, P.R. Mayeux, T.A. Morinelli, Thromboxane, prostaglandin and leukotriene receptors, Annu. Rev. Pharmacol. Toxicol. 29 (1989) 213–239.
[4] A. Sachinidis, M. Flesch, Y. Ko, K. Schror, M. Bohm, R. Dusing, H. Vetter, Thromboxane A2 and vascular smooth muscle cell proliferation, Hypertension 26 (1995) 771–780.
[5] I. Sakuma, S.S. Gross, R. Levi, Positive inotropic effect of the thromboxane analog U-46619 on guinea pig left atrium: mediation by specific receptors and association with increased phosphoinositide turnover, Can. J. Physiol. Pharmacol. 67 (1989) 943–949.
[6] J.L. Mehta, D. Lawson, P. Mehta, T. Saldeen, Increased prostacyclin and thromboxane A2 biosynthesis in atherosclerosis, Proc. Natl. Acad. Sci. USA 85 (1988) 4511–4515.
[7] P. Gresele, H. Deckmyn, G.G. Nenci, J. Vermylen, Thromboxane synthase inhibitors, thromboxane receptor antagonists and dual blockers in thrombotic disorders, Trends Pharmacol. Sci. 12 (1991) 158–163.
[8] R. Collins, C. Baigent, P. Sandercock, R. Peto, Antiplatelet therapy for thromboprophylaxis: the need for careful consideration of the evidence from randomised trials. Antiplatelet Trialists' Collaboration, BMJ 309 (1994) 1215–1217.
[9] A.J. Cayatte, Y. Du, J. Oliver-Krasinski, G. Lavielle, T.J. Verbeuren, R.A. Cohen, The thromboxane receptor antagonist S18886 but not aspirin inhibits atherogenesis in apoE-deficient mice: evidence that eicosanoids other than thromboxane contribute to atherosclerosis, Arterioscler. Thromb. Vasc. Biol. 20 (2000) 1724–1728.
[10] Y. Cheng, S.C. Austin, B. Rocca, B.H. Koller, T.M. Coffman, T. Grosser, J.A. Lawson, G.A. FitzGerald, Role of prostacyclin in the cardiovascular response to thromboxane A2, Science 296 (2002) 539–541.
[11] M. Hirata, Y. Hayashi, F. Ushikubi, Y. Yokota, R. Kageyama, S. Nakanishi, S. Narumiya, Cloning and expression of cDNA for a human thromboxane A2 receptor, Nature 349 (1991) 617–620.
[12] T. Namba, Y. Sugimoto, M. Hirata, Y. Hayashi, A. Honda, A. Watabe, M. Negishi, A. Ichikawa, S. Narumiya, Mouse thromboxane A2 receptor: cDNA cloning, expression and northern blot analysis, Biochem. Biophys. Res. Commun. 184 (1992) 1197–1203.
[13] S.D. Katugampola, A.P. Davenport, Thromboxane receptor density is increased in human cardiovascular disease with evidence for inhibition at therapeutic concentrations by the AT(1) receptor antagonist losartan, Br. J. Pharmacol. 134 (2001) 1385–1392.
[14] T. Ishizuka, K. Suzuki, M. Kawakami, Y. Kawaguchi, T. Hidaka, Y. Matsuki, H. Nakamura, DP-1904, a specific inhibitor of thromboxane A2 synthesizing enzyme, suppresses ICAM-1 expression by stimulated vascular endothelial cells, Eur. J. Pharmacol. 262 (1994) 113–123.
[15] T. Ishizuka, K. Suzuki, M. Kawakami, T. Hidaka, Y. Matsuki, H. Nakamura, Thromboxane A2 receptor blockade suppresses intercellular adhesion molecule-1 expression by stimulated vascular endothelial cells, Eur. J. Pharmacol. 312 (1996) 367–377.
[16] T. Ishizuka, M. Kawakami, T. Hidaka, Y. Matsuki, M. Takamizawa, K. Suzuki, A. Kurita, H. Nakamura, Stimulation with thromboxane A2 (TXA2) receptor agonist enhances ICAM-1, VCAM-1 or ELAM-1 expression by human vascular endothelial cells, Clin. Exp. Immunol. 112 (1998) 464–470.
[17] T. Ishizuka, S. Sawada, K. Sugama, A. Kurita, Thromboxane A2 (TXA2) receptor blockade suppresses monocyte chemoattractant protein-1 (MCP-1) expression by stimulated vascular endothelial cells, Clin. Exp. Immunol. 120 (2000) 71–78.
[18] K. Hanasaki, T. Nakano, H. Arita, Receptor-mediated mitogenic effect of thromboxane A2 in vascular smooth muscle cells, Biochem. Pharmacol. 40 (1990) 2535–2542.
[19] R. Ross, Atherosclerosis—an inflammatory disease, N. Engl. J. Med. 340 (1999) 115–126.
[20] M.O. Pentikainen, R. Oksjoki, K. Oorni, P.T. Kovanen, Lipoprotein lipase in the arterial wall: linking LDL to the arterial extracellular matrix and much more, Arterioscler. Thromb. Vasc. Biol. 22 (2002) 211–217.
[21] M.D. Trip, V.M. Cats, F.J. van Capelle, J. Vreeken, Platelet hyperreactivity and prognosis in survivors of myocardial infarction, N. Engl. J. Med. 322 (1990) 1549–1554.
[22] T. Kobayashi, Y. Tahara, M. Matsumoto, M. Iguchi, H. Sano, T. Murayama, H. Arai, H. Oida, T. Yurugi-Kobayashi, J.K. Yamashita, H. Katagiri, M. Majima, M. Yokode, T. Kita, S. Narumiya, Roles of thromboxane A(2) and prostacyclin in the development of atherosclerosis in apoE-deficient mice, J. Clin. Invest. 114 (2004) 784–794.
[23] M. Sata, A. Saiura, A. Kunisato, A. Tojo, S. Okada, T. Tokuhisa, H. Hirai, M. Makuuchi, Y. Hirata, R. Nagai, Hematopoietic stem cells differentiate into vascular cells that participate in the pathogenesis of atherosclerosis, Nat. Med. 8 (2002) 403–409.
[24] A.S. Plump, J.D. Smith, T. Hayek, K. Aalto-Setala, A. Walsh, J.G. Verstuyft, E.M. Rubin, J.L. Breslow, Severe hypercholesterolemia and atherosclerosis in apolipoprotein E-deficient mice created by homologous recombination in ES cells, Cell 71 (1992) 343–353.
[25] K. Kabashima, T. Murata, H. Tanaka, T. Matsuoka, D.N. Sakata, Yoshida, K. Katagiri, T. Kinashi, T. Tanaka, M. Miyasaka, H. Nagai, F. Ushikubi, S. Narumiya, Thromboxane A2 modulates interaction of dendritic cells and T cells and regulates acquired immunity, Nat. Immunol. 4 (2003) 694–701.
[26] B.M. Schreiber, B.M. Martin, W. Hollander, C. Franzblau, beta-VLDL-induced alterations in growth potentiating activity produced by mononuclear phagocytes, Atherosclerosis 69 (1988) 69–79.
[27] D.L. Thiele, M.L. Eigenbrodt, S.E. Bryde, E.H. Eigenbrodt, P.E. Lipsky, Intestinal graft-versus-host disease is initiated by donor T cells distinct from classic cytotoxic T lymphocytes, J. Clin. Invest. 84 (1989) 1947–1956.
[28] V.I. Rebel, S. Hartnett, G.R. Hill, S.B. Lazo-Kallanian, J.L. Ferrara, C.A. Sieff, Essential role for the p55 tumor necrosis factor receptor in regulating hematopoiesis at a stem cell level, J. Exp. Med. 190 (1999) 1493–1504.
[29] T. Murayama, O.M. Tepper, M. Silver, H. Ma, D.W. Losordo, J.M. Isner, T. Asahara, C. Kalka, Determination of bone marrow-derived endothelial progenitor cell significance in angiogenic growth factor-induced neovascularization in vivo, Exp. Hematol. 30 (2002) 967–972.
[30] Y.R. Su, M.F. Linton, S. Fazio, Rapid quantification of murine ABC mRNAs by real time reverse transcriptase-polymerase chain reaction, J. Lipid Res. 43 (2002) 2180–2187.
[31] T. Murayama, M. Yokode, H. Kataoka, T. Imabayashi, H. Yoshida, H. Sano, S. Nishikawa, T. Kita, Intraperitoneal administration of anti-c-fms monoclonal antibody prevents initial events of atherogenesis but does not reduce the size of advanced lesions in apolipoprotein E-deficient mice, Circulation 99 (1999) 1740–1746.
[32] H. Sano, T. Sudo, M. Yokode, T. Murayama, H. Kataoka, N. Takakura, S. Nishikawa, S.I. Nishikawa, T. Kita, Functional blockade of platelet-derived growth factor receptor-beta but not of receptor-alpha prevents vascular smooth muscle cell accumulation in fibrous cap lesions in apolipoprotein E-deficient mice, Circulation 103 (2001) 2955–2960.

[33] Y. Xu, H. Arai, X. Zhuge, H. Sano, T. Murayama, M. Yoshimoto, T. Heike, T. Nakahata, S.I. Nishikawa, T. Kita, M. Yokode, Role of bone marrow-derived progenitor cells in cuff-induced vascular injury in mice, Arterioscler. Thromb. Vasc. Biol. 24 (2004) 477–482.
[34] A. Nicoletti, S. Kaveri, G. Caligiuri, J. Bariety, G.K. Hansson, Immunoglobulin treatment reduces atherosclerosis in apoE knockout mice, J. Clin. Invest. 102 (1998) 910–918.
[35] H. Ma, A. Hara, C.Y. Xiao, Y. Okada, O. Takahata, K. Nakaya, Y. Sugimoto, A. Ichikawa, S. Narumiya, F. Ushikubi, Increased bleeding tendency and decreased susceptibility to thromboembolism in mice lacking the prostaglandin E receptor subtype EP(3), Circulation 104 (2001) 1176–1180.
[36] R.A. Coleman, W.L. Smith, S. Narumiya, International Union of Pharmacology classification of prostanoid receptors: properties, distribution, and structure of the receptors and their subtypes, Pharmacol. Rev. 46 (1994) 205–229.
[37] S.I. Murota, M. Kawamura, I. Morita, Transformation of arachidonic acid into thromboxane B2 by the homogenates of activated macrophages, Biochim. Biophys. Acta 528 (1978) 507–511.
[38] R. Nusing, V. Ullrich, Immunoquantitation of thromboxane synthase in human tissues, Adv. Prostagl. Thromb. Leukot. Res. 21A (1991) 307–310.
[39] Y. Tone, A. Miyata, S. Hara, S. Yukawa, T. Tanabe, Abundant expression of thromboxane synthase in rat macrophages, FEBS Lett. 340 (1994) 241–244.
[40] K.M. Egan, M. Wang, M.B. Lucitt, A.M. Zukas, E. Pure, J.A. Lawson, G.A. FitzGerald, Cyclooxygenases, thromboxane, and atherosclerosis: plaque destabilization by cyclooxygenase-2 inhibition combined with thromboxane receptor antagonism, Circulation 111 (2005) 334–342.
[41] V.R. Babaev, L. Ding, J. Reese, J.D. Morrow, M.D. Breyer, S.K. Dey, S. Fazio, M.F. Linton, Cyclooxygenase-1 deficiency in bone marrow cells increases early atherosclerosis in apolipoprotein E- and low-density lipoprotein receptor-null mice, Circulation 113 (2006) 108–117.
[42] A.W. Ashton, J.A. Ware, Thromboxane A2 receptor signaling inhibits vascular endothelial growth factor-induced endothelial cell differentiation and migration, Circ. Res. 95 (2004) 372–379.
[43] L. Belhassen, G. Pelle, J.L. Dubois-Rande, S. Adnot, Improved endothelial function by the thromboxane A2 receptor antagonist S 18886 in patients with coronary artery disease treated with aspirin, J. Am. Coll. Cardiol. 41 (2003) 1198–1204.

THE JOURNAL OF BIOLOGICAL CHEMISTRY VOL 281, NO 41, pp 31164–31172, October 13, 2006

Nardilysin Enhances Ectodomain Shedding of Heparin-binding Epidermal Growth Factor-like Growth Factor through Activation of Tumor Necrosis Factor-α-converting Enzyme*

Received for publication, February 10, 2006, and in revised form, August 4, 2006 Published, JBC Papers in Press, August 21, 2006, DOI 10.1074/jbc.M601316200

Eiichiro Nishi[‡1], **Yoshinori Hiraoka**[‡], **Kazuhiro Yoshida**[§], **Katsuya Okawa**[¶], **and Toru Kita**[§]

From the [‡]*Molecular Pathology and* [¶]*Biomolecular Characterization Unit, Horizontal Medical Research Organization, and the* [§]*Department of Cardiovascular Medicine, Graduate School of Medicine, Kyoto University, Kyoto 606-8507, Japan*

Like other members of the epidermal growth factor family, heparin-binding epidermal growth factor-like growth factor (HB-EGF) is synthesized as a transmembrane protein that can be shed enzymatically to release a soluble growth factor. Ectodomain shedding is essential to the biological functions of HB-EGF and is strictly regulated. However, the mechanism that induces the shedding remains unclear. We have recently identified nardilysin (*N*-arginine dibasic convertase (NRDc)), a metalloendopeptidase of the M16 family, as a protein that specifically binds HB-EGF (Nishi, E., Prat, A., Hospital, V., Elenius, K., and Klagsbrun, M. (2001) *EMBO J.* 20, 3342–3350). Here, we show that NRDc enhances ectodomain shedding of HB-EGF. When expressed in cells, NRDc enhanced the shedding in cooperation with tumor necrosis factor-α-converting enzyme (TACE; ADAM17). NRDc formed a complex with TACE, a process promoted by phorbol esters, general activators of ectodomain shedding. NRDc enhanced TACE-induced HB-EGF cleavage in a peptide cleavage assay, indicating that the interaction with NRDc potentiates the catalytic activity of TACE. The metalloendopeptidase activity of NRDc was not required for the enhancement of HB-EGF shedding. Notably, a reduction in the expression of NRDc caused by RNA interference was accompanied by a decrease in ectodomain shedding of HB-EGF. These results indicate the essential role of NRDc in HB-EGF ectodomain shedding and reveal how the shedding is regulated by the modulation of sheddase activity.

Ectodomain shedding is an irreversible post-translational modification that releases the extracellular domain of membrane-anchored proteins through proteolysis. A broad spectrum of membrane proteins are susceptible to ectodomain shedding. Ectodomain shedding of most proteins occurs constitutively in resting cells, but can be rapidly and markedly induced by cell activation. However, the mechanism that induces shedding remains unclear (1–4).

Heparin-binding epidermal growth factor-like growth factor (HB-EGF)[2] is synthesized as a transmembrane protein (pro-HB-EGF) that can be shed proteolytically to release a soluble growth factor (5–8). Metalloproteinases have been implicated as sheddases of pro-HB-EGF because various metalloproteinase inhibitors inhibit HB-EGF ectodomain shedding efficiently. MMP3 (matrix metalloproteinase-3), MMP7, ADAM9 (a disintegrin and metalloproteinase-9), ADAM10, ADAM12, and ADAM17 (tumor necrosis factor-α-converting enzyme (TACE)) have all been suggested as the proteases responsible (9–14). Ectodomain shedding of pro-HB-EGF is induced by various stimuli, including phorbol esters, calcium ionophore, and lysophosphatidic acid (6, 15, 16). With respect to the mechanism of the induction, however, very little is known.

Ectodomain shedding of HB-EGF is indispensable for G-protein-coupled receptor-induced epidermal growth factor receptor (EGFR) transactivation, which plays critical roles in biological consequences of G-protein-coupled receptor activation (17). The physiological significance of HB-EGF ectodomain shedding was further underscored by the findings that knock-in mice harboring an uncleavable mutant construct of HB-EGF show phenotypes very similar to those of HB-EGF knock-out mice (*e.g.* hypertrophied cardiac valve and dilated heart) and that knock-in mice with the soluble mutant have even more severe phenotypes (18–20). Notably, a similarly defective valvulogenesis was observed in both EGFR- and TACE-deficient mice, suggesting that HB-EGF-induced EGFR activation and TACE-induced HB-EGF shedding are required for valvulogenesis (19, 21). In other words, ectodomain shedding of pro-HB-EGF is required for the activation of EGFR by HB-EGF. The same conclusion was obtained in a study that showed that most of the biological effects of EGFR ligands in cell culture are blocked by metalloprotease inhibitors (22).

* This work was supported by Special Coordination Funds for Promoting Science and Technology Research Grants 16590680 and 18590809 from the Ministry of Education, Culture, Sports, Science, and Technology of Japan, by a Japan Heart Foundation research grant, by the Takeda Science Foundation, and by the Kanae Foundation for Life & Socio-Medical Science. The costs of publication of this article were defrayed in part by the payment of page charges. This article must therefore be hereby marked "*advertisement*" in accordance with 18 U.S.C. Section 1734 solely to indicate this fact.

[1] To whom correspondence should be addressed: Molecular Pathology Unit, Horizontal Medical Research Organization, Graduate School of Medicine, Kyoto University, 54 Shogoin-Kawahara-Cho, Sakyo-Ku, Kyoto 606-8507, Japan. Tel.: 81-75-751-3187; Fax: 81-75-751-3203; E-mail: nishi@kuhp.kyoto-u.ac.jp.

[2] The abbreviations used are: HB-EGF, heparin-binding epidermal growth factor-like growth factor; TACE, tumor necrosis factor-α-converting enzyme; EGFR, epidermal growth factor receptor; NRDc, *N*-arginine dibasic convertase (nardilysin); HA, hemagglutinin; AP, alkaline phosphatase; siRNAs, small interfering RNAs; GAPDH, glyceraldehyde-3 phosphate dehydrogenase; MALDI-TOF-MS, matrix-assisted laser desorption ionization time-of-flight mass spectrometry; PMA, phorbol 12-myristate 13-acetate.

We have previously shown that nardilysin (*N*-arginine dibasic convertase (NRDc)) binds specifically to HB-EGF among EGF family members (23). NRDc was originally identified as a dibasic selective metalloendopeptidase of the M16 family (24, 25). Expression of the enzyme is widespread and especially high in testis, heart, and skeletal muscle (26). NRDc is expressed mainly in the cytoplasm, but interestingly, it is also exported out of cells and distributed on the cell surface, although it has no apparent signal peptide sequence (27–29). While examining the biological significance of the binding of NRDc to pro-HB-EGF, we found that NRDc enhances ectodomain shedding of the growth factor. Here, we demonstrate that a metalloendopeptidase, NRDc, potentiates the catalytic activity of TACE and enhances ectodomain shedding of HB-EGF.

EXPERIMENTAL PROCEDURES

Plasmids—cDNA encoding human NRDc (Met^{50}–Lys^{1150}, completely matching GenBank™ accession number BC008775) was cloned into pcDNA3.1/V5-His (Invitrogen) to generate pcDNA3.1-hNRDc-V5. The cDNA of human NRDc C-terminally tagged with FLAG was cloned into pcDNA3 and pFastBac1 (Invitrogen) to generate pcDNA3-hNRDc-FLAG and pFastBac1-hNRDc-FLAG, respectively. A cDNA encoding an enzymatically inactive mutant of human NRDc was obtained by substituting the Glu^{235} codon (GAG) with an Ala codon (GCG) using the PCR technique. The full-length human TACE cDNA was cloned into pME18S to generate pME18S-hTACE. The expression plasmid for hemagglutinin (HA)-tagged HB-EGF was described previously (30). The expression plasmid for alkaline phosphatase (AP)-tagged HB-EGF (31) was a gift from S. Higashiyama.

Small Interfering RNAs (siRNAs)—The sequences for siRNA duplexes were as follows: NRDc-1, 5′-GGGUAGUGAUAAUGCCUCAACUGAU-3′; NRDc-2, 5′-GACUACUUAGCUGAGUUCAAUUCCA-3′; Control-2, 5′-ACGUGACACGUUCGGAGAA-3′. NRDc-1 and NRDc-2 are Stealth™ siRNA duplex oligoribonucleotides synthesized by Invitrogen. Control-2 is a control (nonsilencing) siRNA purchased from Qiagen Inc. Control-1 is a Stealth RNAi negative control duplex with medium GC content purchased from Invitrogen, the sequence of which is not available to the public.

Antibodies and Reagents—The antibodies were from the following sources: anti-HA tag antibody HA11, Covance; anti-V5 tag antibody, Invitrogen; anti-FLAG tag antibody M2, Sigma; anti-TACE antibodies (C-15 and H-300), Santa Cruz Biotechnology, Inc.; anti-TACE antibody (clone 111633), R&D Systems; anti-HB-EGF antibody, Calbiochem; and anti-glyceraldehyde-3 phosphate dehydrogenase (GAPDH) antibody, Research Diagnostics, Inc. Anti-TACE antibody 41 (used for immunoprecipitation) was a gift from M. E. Milla. Mouse anti-NRDc monoclonal antibody 23 was raised against recombinant human NRDc in our laboratory. Recombinant NRDc was synthesized using the Bac-to-Bac baculovirus expression system (Invitrogen). Briefly, pFastBac1-hNRDc-FLAG was introduced into DH10Bac competent cells to isolate recombinant bacmid DNA. Sf9 cells were transfected with the bacmid DNA, and the recombinant baculovirus-containing supernatant was harvested. Sf9 cells inoculated with the recombinant virus were lysed in lysis buffer containing 50 mM Tris-HCl (pH 7.4), 150 mM NaCl, 2 μg/ml leupeptin, 0.2 mg/ml Pefabloc SC^{PLUS} (Roche Applied Science), and 1% Nonidet P-40, and the total cell lysate was loaded onto an anti-FLAG antibody M2 affinity gel column (Sigma) and eluted with FLAG peptide (100 μg/ml). Recombinant TACE was purchased from R&D Systems.

Cells and Transfections—COS-7 and 293T cells were grown in Dulbecco's modified Eagle's medium containing 10% fetal calf serum. MKN45 cells were grown in RPMI 1640 medium containing 10% fetal calf serum. Transfections were carried out using FuGENE 6 (Roche Applied Science) for plasmids and siFECTOR (B-Bridge International Inc.) for siRNA according to the manufacturers' instructions. CHO-K1 cells stably expressing HA-HB-EGF (CHO-K1-HA-HB-EGF cells) and AP-HB-EGF (CHO-K1-AP-HB-EGF cells) were selected in nutrient mixture F-12 containing 10% fetal calf serum and 500 mg/ml G418, respectively. Clones of CHO-K1-HA-HB-EGF cells were tested for HA-HB-EGF expression by Western blotting with anti-HA antibody. CHO-K1-AP-HB-EGF cells were sorted by the expression of AP-HB-EGF (using anti-AP antibody) using a FACSAria flow cytometer (BD Biosciences).

Western Blot Analysis—Cells were lysed in lysis buffer containing 10 mM Tris-HCl (pH 7.4), 150 mM NaCl, 1% Nonidet P-40, and protease inhibitor mixture (Roche Applied Science). Cell lysates were separated by SDS-PAGE and transferred to nitrocellulose filters. After blocking with 5% nonfat milk in 10 mM Tris-HCl (pH 7.4), 150 mM NaCl, and 0.05% Tween 20, filters were incubated with primary antibodies, followed by horseradish peroxidase-conjugated secondary antibodies. The immobilized peroxidase activity was detected with the enhanced chemiluminescence system (ECL, Amersham Biosciences).

Immunoprecipitation—Cell lysates were incubated with the appropriate antibodies, and immune complexes were collected with protein G-Sepharose beads.

Pulldown Assay—Recombinant NRDc (FLAG-tagged at the C terminus; 11 μg/ml), TACE (10 μg/ml), and HB-EGF (2.8 μg/ml) were mixed in 50 mM Tris-HCl (pH 8.9), 1 mM $CaCl_2$, and 15 mM $ZnCl_2$. The mixture was incubated with anti-FLAG antibody-conjugated beads for 4 h, followed by extensive washes, and the precipitates were subjected to SDS-PAGE and blotted with anti-TACE antibody (clone 111633).

Peptide Cleavage and Molecular Mass Analysis—The fluorescence-quenching peptide substrate corresponding to the cleavage site of HB-EGF (2-(*N*-methylamino)benzoyl-LPVENRLYK(2,4-dinitrophenyl)D-Arg-amide) was synthesized by Peptide Institute, Inc. (Osaka, Japan). Peptide substrate for the HB-EGF cleavage site (GLSLPVENRLYTYD) used for molecular mass analysis was synthesized by Hokkaido System Science Co., Ltd. (Hokkaido, Japan). *In vitro* peptide cleavage assays were performed in 25 mM Tris-HCl (pH 9.0) and 2.5 μM $ZnCl_2$. Molecular mass analyses of peptides were performed by matrix-assisted laser desorption ionization time-of-flight mass spectrometry (MALDI-TOF-MS) using an Ultraflex TOF/TOF system (Bruker Daltonics Inc.).

Immunocytochemistry—Cells were fixed with 50% acetone and 50% methanol. Nonspecific staining was blocked with blocking solution (5% donkey and 1% sheep sera in phosphate-

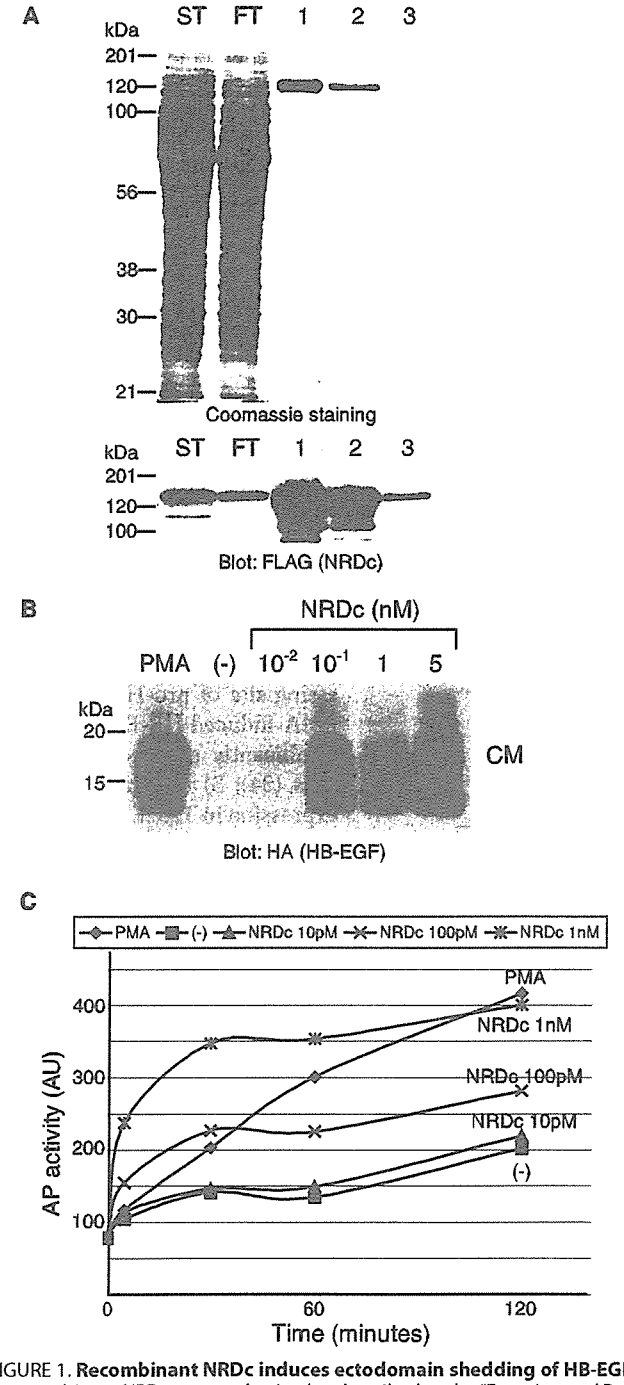

FIGURE 1. **Recombinant NRDc induces ectodomain shedding of HB-EGF.** *A*, recombinant NRDc was synthesized as described under "Experimental Procedures." The total cell lysate of Sf9 cells inoculated with a recombinant baculovirus (starting material (*ST*)) was loaded onto an anti-FLAG antibody-conjugated gel column and eluted with FLAG peptide. The starting material, the flow-through (*FT*), and three fractions of the eluate (*1*, *2*, and *3*) were separated by SDS-PAGE and subjected to either Coomassie Blue staining (*upper panel*) or Western blotting with anti-FLAG antibody (*lower panel*). *B*, CHO-K1-HA-HB-EGF cells were incubated with the indicated concentrations of recombinant NRDc or 100 nM PMA for 4 h. The soluble HB-EGF released in the conditioned medium (*CM*) was partially purified with heparin-Sepharose beads and separated by SDS-PAGE, followed by Western blotting with anti-HA antibody. Molecular masses are indicated to the left. Comparable data were obtained in three independent experiments, and a representative gel is shown. *C*, CHO-K1-AP-HB-EGF cells were incubated with recombinant NRDc or PMA. The AP activity in the conditioned medium was measured at the indicated time points. Similar results were obtained in two independent experiments, and a representative result is shown. *AU*, arbitrary units.

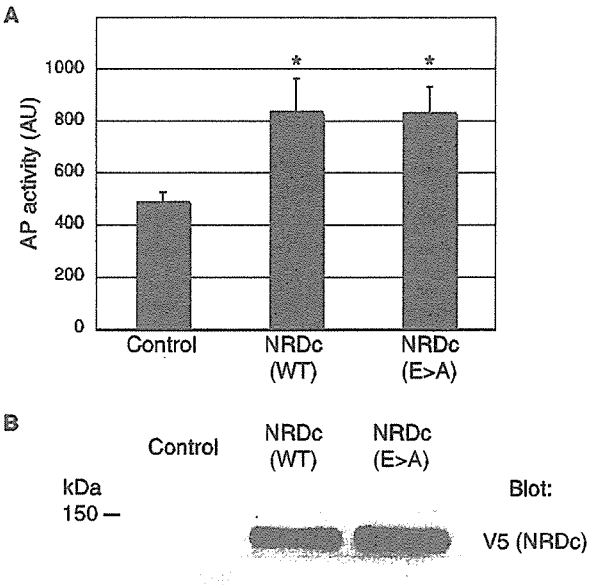

FIGURE 2. **Expression of NRDc induces ectodomain shedding of HB-EGF, and NRDc enzymatic activity is not required for the induction.** *A*, an expression vector encoding AP-HB-EGF was cotransfected into COS-7 cells with a control vector, an expression vector for wild-type NRDc-V5 (*WT*), or an enzymatically inactive mutant of NRDc-V5 (E235A (*E* > *A*)). The culture medium was changed to Dulbecco's modified Eagle's medium with 0.1% bovine serum albumin 20 h post-transfection. The AP activity in the conditioned medium was measured after an additional 4 h of incubation. Data represent the means ± S.E. for five independent experiments. *, $p < 0.04$ (Student's *t* test). *AU*, arbitrary units. *B*, total cell lysates of transfected cells were collected, and NRDc expression was analyzed by Western blotting with anti-V5 antibody.

buffered saline). The cells were incubated overnight at 4 °C with a proper dilution of primary antibodies in blocking solution, followed by the respective secondary antibodies for 1 h at room temperature. The stained cells were observed with a Zeiss LSM 510 META laser scanning confocal microscope or a Zeiss Axioskop 2 fluorescence microscope. Collected data were exported as eight-bit TIFF files and processed using ImageJ Version 1.30 (available at rsb.info.nih.gov/ij/).

RESULTS

NRDc Induces Ectodomain Shedding of HB-EGF—To define the biological significance of the binding of NRDc to pro-HB-EGF, we examined the effects of NRDc on HB-EGF ectodomain shedding. To facilitate detection of shed soluble HB-EGF in the conditioned medium, two N-terminally tagged pro-HB-EGFs, HA-HB-EGF (30) and AP-HB-EGF (31), were used. Recombinant NRDc tagged with FLAG at the C terminus was produced in a baculovirus-insect cell system and purified by immunoaffinity chromatography with anti-FLAG antibody. Coomassie Blue staining of eluted fractions showed very high purity of the recombinant NRDc (Fig. 1*A*), and the enzymatic activity of NRDc was confirmed by conducting a cleavage assay with a fluorescence-quenching peptide substrate (2-(*N*-methylamino)benzoyl-GGFLRRVGK(2,4-dinitrophenyl)-amide; fluorescence intensity at 340/430 nm of 38,740 arbitrary units at 177 μM recombinant NRDc and of 1581 arbitrary units at the same concentration of the enzymatically inactive mutant of NRDc). Treatment of CHO-K1-HA-HB-EGF cells with recombinant

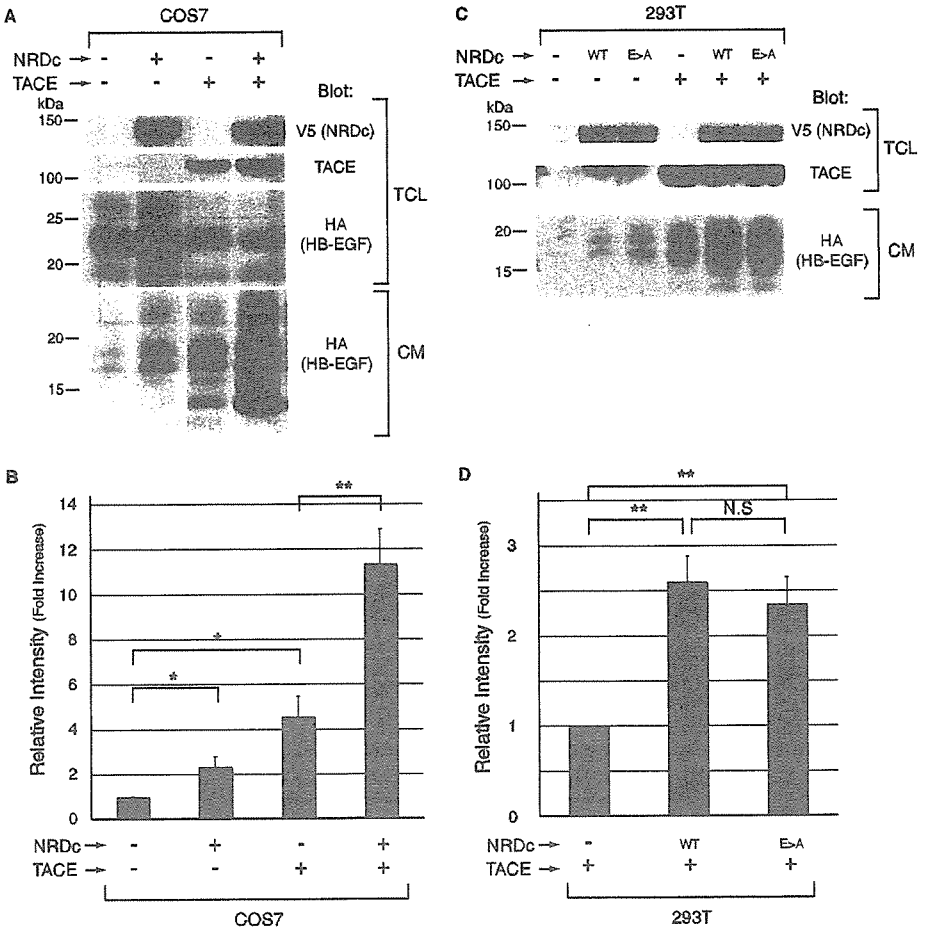

FIGURE 3. **NRDc and TACE cooperate to enhance ectodomain shedding of HB-EGF.** *A*, HA-HB-EGF was transiently cotransfected into COS-7 cells with combinations of expression vectors for NRDc-V5 and TACE as indicated. The culture medium of transfected cells was changed to Dulbecco's modified Eagle's medium with 0.1% bovine serum albumin 20 h post-transfection. The conditioned medium (*CM*) and total cell lysates (*TCL*) were collected after an additional 4 h of incubation. Western blot analysis with anti-V5 (NRDc), anti-TACE (C-15), and anti-HA (HB-EGF) antibodies was conducted for the total cell lysates. Blotting with anti-HA antibody (HB-EGF) was carried out for the soluble HB-EGF released in the conditioned medium, which was partially purified with heparin-Sepharose beads. *B*, shown are the results from the quantification of shed HB-EGF in the five independent experiments of *A*. A densitometric analysis was performed using ImageJ Version 1.30. The ratio was arbitrarily set at 1 in control vector-transfected cells (*first lane* in *A*). Data represent the means ± S.E. *, $p < 0.05$ (Student's *t* test); **, $p < 0.005$. *C*, HA-HB-EGF was transiently cotransfected into 293T cells with combinations of expression vectors for wild-type NRDc-V5 (*WT*), an enzymatically inactive mutant of NRDc-V5 (E235A (*E>A*)), and TACE as indicated. The conditioned medium and total cell lysates were collected, and Western blot analysis was performed as described for *A*. *D*, shown are the results from the quantification of shed HB-EGF in the seven independent experiments of *C*. A densitometric analysis of HB-EGF released from cells expressing TACE (*C*, *fourth lane*), TACE plus NRDc (*C*, *fifth lane*), and TACE plus NRDc(E235A) (*C*, *sixth lane*) was done. The ratio was arbitrarily set at 1 in the TACE-transfected cells (*C*, *fourth lane*). Data represent the means ± S.E. **, $p < 0.005$ (Student's *t* test); *N.S*, not significant.

NRDc induced ectodomain shedding of HB-EGF in a dose-dependent manner (Fig. 1*B*). Recombinant NRDc also enhanced HB-EGF shedding in CHO-K1-AP-HB-EGF cells in a similar manner (Fig. 1*C*). Interestingly, NRDc induced HB-EGF shedding more rapidly compared with phorbol 12-myristate 13-acetate (PMA) in the early time course.

Although NRDc is found in conditioned media, it is found primarily in the cytosol and on the cell surface (27, 29). Thus, we examined the effect of coexpression of NRDc and AP-HB-EGF on HB-EGF shedding. Cells expressing NRDc released significantly more AP activity in the conditioned medium compared with cells transfected with an empty vector (Fig. 2*A*). The enzymatically inactive mutant of NRDc (E235A) also enhanced HB-EGF shedding (Fig. 2*A*), indicating that the metalloendopeptidase activity of NRDc is not required for the enhancement of HB-EGF shedding. Western blot analysis showed a comparable expression level of NRDc and the inactive mutant of NRDc (Fig. 2*B*). These results indicate that NRDc does not directly cleave HB-EGF, suggesting that it modulates shedding by regulating other pathways of the mechanism.

NRDc and TACE Cooperate to Enhance Ectodomain Shedding of HB-EGF—Several lines of evidence indicate that TACE/ADAM17, which was originally identified as a sheddase for tumor necrosis factor-α (32, 33), plays an essential role in ectodomain shedding of HB-EGF. 1) Recombinant TACE cleaves the peptide corresponding to the processing site of pro-HB-EGF (14); 2) PMA-induced HB-EGF shedding is significantly reduced in TACE$^{-/-}$ cells (34); 3) restoration of TACE expression in TACE$^{-/-}$ cells results in a significant increase in HB-EGF shedding (14); and 4) HB-EGF-null mice, knock-in mice with an uncleavable mutant of HB-EGF, and TACE-null mice show a similar heart valve phenotype (18–20). To determine whether NRDc has a cooperative effect on TACE activity, cotransfection experiments were performed in COS-7 cells, and HB-EGF ectodomain shedding was evaluated by Western blotting for HB-EGF released into the conditioned medium. The transfection of only NRDc had a significant but relatively small effect on HB-EGF shedding (2.3-fold increase) (Fig. 3, *A*, compare the *first* and *second lanes*; and *B*, compare the *first* and *second bars*), compatible with the result in Fig. 2*A*. However, coexpression of NRDc and TACE dramatically enhanced HB-EGF ectodomain shedding compared with expression of TACE alone (Fig. 3, *A*, compare the *third* and *fourth lanes*; and *B*, compare the *third* and *fourth bars*). A quantitative analysis of shed HB-EGF in the five independent experiments clearly showed that the effect of the combination was not additive, but was synergistic (2.3-fold increase by NRDc, 4.5-fold increase by TACE, and 11.3-fold increase by NRDc and TACE) (Fig. 3*B*). We performed the same cotransfection experiments in a different cell line (293T cells) and obtained very similar results (Fig. 3*C*). The synergistic effect of the enzymatically inactive mutant of NRDc on TACE-induced

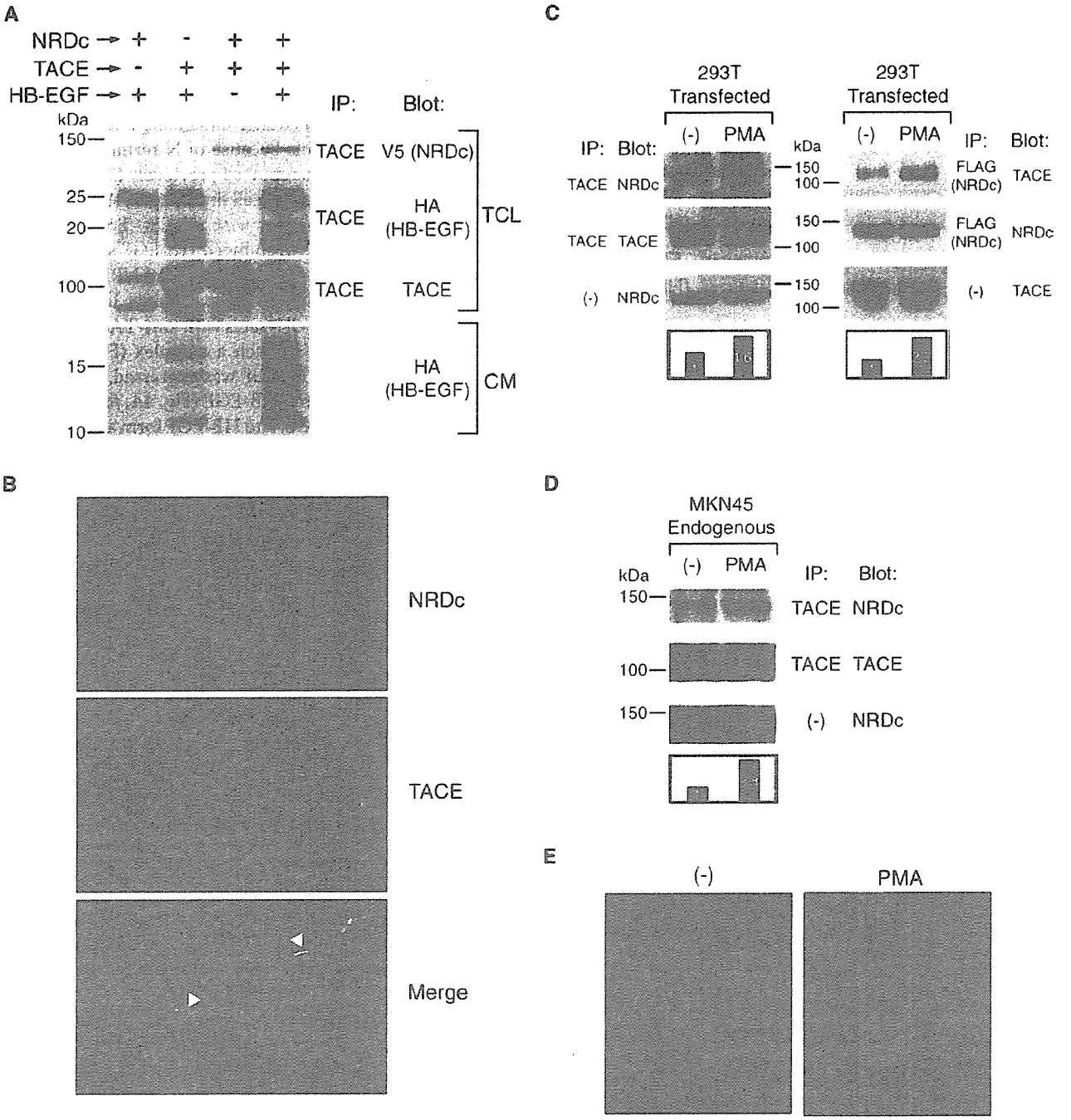

FIGURE 4. **NRDc and TACE form a complex, a process enhanced by PMA.** *A*, 293T cells were transfected with combinations of expression vectors for NRDc-V5, TACE, and HA-HB-EGF as indicated. The conditioned medium (*CM*) and total cell lysates (*TCL*) were collected as described in the legend to Fig. 3*A*. Immunoprecipitation (*IP*) with anti-TACE antibody 41 was done for the total cell lysates, and precipitates were blotted with anti-V5 (NRDc), anti-HA (HB-EGF), and anti-TACE (C-15) antibodies. The soluble HB-EGF released in the conditioned medium was detected as described in the legend to Fig. 1*B*. Comparable data were obtained in three independent experiments, and a representative gel is shown. *B*, 293T cells were transiently transfected with expression vectors for NRDc-V5 and TACE, fixed, and stained with anti-TACE (H-300; *green*) and anti-V5 (*red*) antibodies. A mixture of Alexa Fluor 594-conjugated donkey anti-mouse IgG and Alexa Fluor 488-conjugated donkey anti-rabbit IgG was used as secondary antibodies. Stained cells were visualized by confocal microscopy. *Arrowheads* show the co-localization of NRDc and TACE. *C*, 293T cells transfected with expression vectors for NRDc-V5 and TACE (*left panel*) or NRDc-FLAG and TACE (*right panel*) were incubated in the absence or presence of PMA for 2 h. Total cell lysates were collected, and immunoprecipitation with anti-TACE antibody 41 (*left panel*) or anti-FLAG antibody M2 (*right panel*) was carried out. The precipitates and total cell lysates were separated by SDS-PAGE and blotted with anti-NRDc antibody 23 or anti-TACE antibody (C-15). A quantitative analysis of the coprecipitated proteins (*upper panels*) by densitometry is shown (*fourth left* and *right panels*). The ratio was arbitrarily set at 1 in the cells treated without PMA (*first lane*) and shown in the *bars*. Similar results were obtained in three independent experiments, and a representative result is shown. *D*, MKN45 cells (a gastric cancer cell line) were incubated in the absence or presence of PMA for 2 h. The total cell lysates were collected and immunoprecipitated with anti-TACE antibody 41, and Western blotting was conducted as described for *C*. Comparable results were obtained in three independent experiments, and a representative result is shown. *E*, MKN45 cells were incubated in the absence (*left panel*) or presence (*right panel*) of PMA for 2 h, fixed, and stained with anti-NRDc antibody 23. Alexa Fluor 594-conjugated donkey anti-mouse IgG was used as secondary antibody, and the nucleus was subsequently stained with 4′,6-diamidino-2-phenylindole. Stained cells were visualized by fluorescence microscopy.

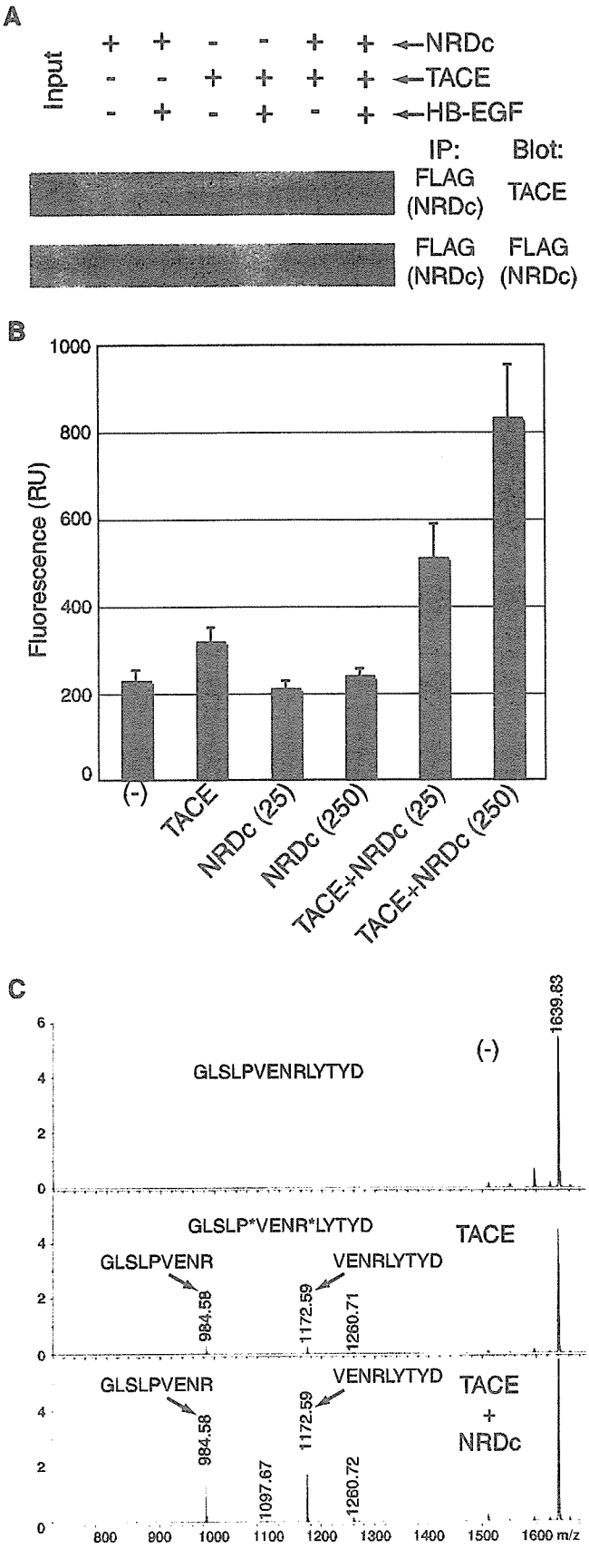

HB-EGF shedding was also examined in 293T cells. The inactive NRDc mutant showed a similar enhancing effect on HB-EGF shedding compared with wild-type NRDc (Fig. 3, *C* and *D*), indicating that the metalloendopeptidase activity of NRDc is not required for the shedding-enhancing effect of NRDc. HB-EGF has multiple forms because of N-terminal heterogeneity and *O*-glycosylation as reported previously (35) and shows different patterns in different cell lines (Fig. 3, *A* and *C*).

NRDc Forms a Complex with TACE—To investigate how NRDc potentiates TACE-induced HB-EGF shedding, the formation of a complex between TACE and NRDc was examined by conducting coprecipitation experiments. Immunoprecipitation of cotransfected cell lysates with anti-TACE antibody confirmed the formation of such a complex (Fig. 4*A*, *third* and *fourth lanes*). When HB-EGF was expressed, anti-TACE antibody also coprecipitated HB-EGF (Fig. 4*A*, *fourth lane*) , indicating that NRDc, TACE, and HB-EGF form a complex. Immunocytochemical staining of cotransfected cells showed a partial co-localization of TACE and NRDc on the plasma membrane (Fig. 4*B*), supporting the results of coprecipitation.

PMA Treatment Enhances the Formation of a Complex between NRDc and TACE—Ectodomain shedding of most proteins occurs constitutively in resting cells, but can be dramatically induced by cell activation (1, 36). However, TACE processing and expression levels are not increased by cell activation (32, 37). To examine whether the interaction of NRDc and TACE is involved in the regulation of induced HB-EGF shedding, the effect of PMA, a general activator of ectodomain shedding, on NRDc·TACE complex formation was examined. In 293T cells transfected with NRDc and TACE, immunoprecipitation with anti-TACE antibody demonstrated that PMA stimulation increased the engagement of NRDc with TACE (by 1.6-fold as determined by densitometry), whereas PMA did not affect the total amount of TACE and NRDc (Fig. 4*C*, *left panels*). To confirm the effect of PMA through a reciprocal immunoprecipitation, cells were transfected with NRDc-FLAG and TACE, followed by immunoprecipitation with anti-FLAG antibody. In this experimental setting, PMA also enhanced the formation of a complex between NRDc and TACE (by 2.2-fold) (Fig. 4*C*, *right panels*). Furthermore, PMA accelerated the process of endogenous proteins in MKN45 cells (by 2.8-fold), a gastric cancer cell line (Fig. 4*D*). NRDc is expressed primarily in the cytoplasm, but it is also found on the cell surface (27–29). Immunocytochemistry of transfected cells suggested that

FIGURE 5. **TACE is activated by direct binding to NRDc.** *A*, recombinant NRDc FLAG-tagged at the C terminus (11 μg/ml), TACE (10 μg/ml), and HB-EGF (2.8 μg/ml) were mixed as indicated. The mixture was incubated with anti-FLAG antibody-conjugated beads for 4 h and washed extensively, and the precipitates were blotted with anti-TACE antibody (clone 111633; *upper panel*) or anti-FLAG antibody (*lower panel*). *Input*, total input of TACE. *IP*, immunoprecipitation. *B*, NRDc potentiated the catalytic activity of TACE. A fluorescence-quenching peptide substrate corresponding to the cleavage site of HB-EGF (2-(*N*-methylamino)-benzoyl-LPVENRLYK(2,4-dinitrophenyl)D-Arg-amide; 250 mM) was incubated with recombinant TACE (5 μg/ml) and NRDc (25 or 250 μg/ml) as indicated. After 15 h at 37 °C, the fluorescence intensity at 340/430 nm was measured. Data represent the means ± S.D. for three independent experiments. *AU*, arbitrary units. *C*, the HB-EGF cleavage site was determined by MALDI-TOF-MS. A peptide representing the cleavage site of HB-EGF was incubated with TACE (25 μg/ml) in the absence or presence of NRDc (100 μg/ml) for 15 h at 37 °C. Samples were analyzed by MALDI-TOF-MS.

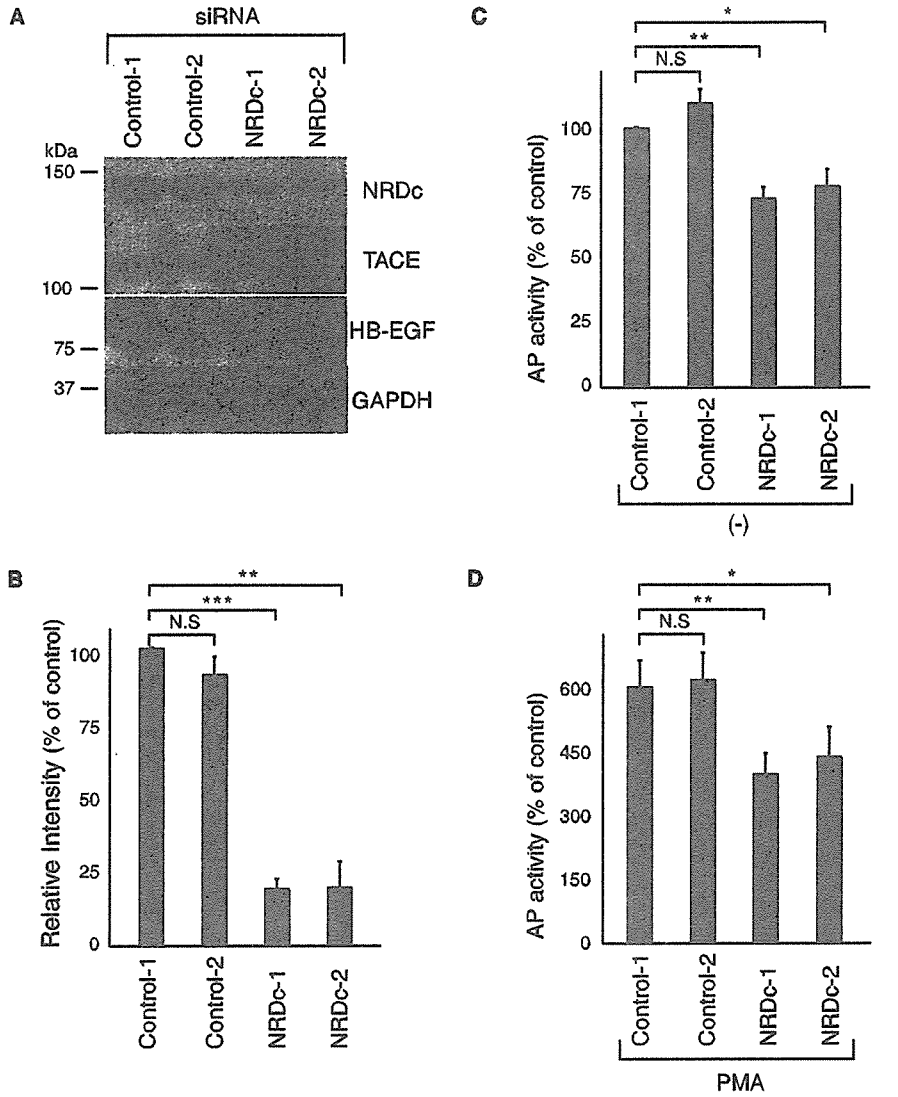

FIGURE 6. **Inhibition of NRDc expression results in decreased shedding of HB-EGF.** AP-HB-EGF was cotransfected into COS-7 cells with either 20 nM control siRNA (Control-1 or Control-2) or NRDc siRNA (NRDc-1 or NRDc-2). The culture medium was changed to fresh medium with 0.1% bovine serum albumin after 48 h, and total cell lysates and the conditioned medium were collected after an additional 5 h of incubation in the absence or presence of PMA (100 nM). *A*, NRDc, TACE, AP-HB-EGF, and GAPDH expression in cells incubated without PMA was analyzed by Western blotting with mouse anti-NRDc monoclonal antibody 23 and anti-TACE (C-15), anti-HB-EGF, and anti-GAPDH antibodies, respectively. *B*, the inhibitory effects of siRNAs on NRDc protein expression (normalized to GAPDH expression) were evaluated by densitometry. The level was arbitrarily set at 100% in cells transfected with Control-1 siRNA. Data represent the means ± S.E. ($n = 7$ for Control-1, $n = 6$ for Control-2 and NRDc-1, and $n = 5$ for NRDc-2). **, $p < 0.005$ (Student's t test); ***, $p < 0.0005$; *N.S*, not significant. *C* and *D*, the AP activity in the conditioned medium collected from cells treated in the absence and presence of PMA, respectively, was measured. The level was arbitrarily set at 100% in Control-1 siRNA-transfected cells treated without PMA. Data represent the means ± S.E. (*C*, $n = 7$ for Control-1, $n = 6$ for Control-2 and NRDc-1, and $n = 5$ for NRDc-2; *D*, $n = 5$ for Control-1, $n = 4$ for Control-2 and NRDc-1, and $n = 3$ for NRDc-2). *, $p < 0.05$ (Student's t test); **, $p < 0.005$; *N.S*, not significant. Note that the scale of the *y axis* is different in *C* and *D*.

NRDc and TACE form a complex mainly on the plasma membrane (Fig. 4*B*). Therefore, we examined the effect of PMA on the distribution of endogenous NRDc in MKN45 cells. Immunofluorescence staining with anti-NRDc antibody showed that PMA increased NRDc expression on the plasma membrane (Fig. 4*E*). These results indicate that NRDc plays a central role in the regulation of induced ectodomain shedding through the translocation and formation of a complex with TACE.

TACE Catalytic Activity Is Enhanced by Direct Binding to NRDc—Pulldown assays verified that NRDc and TACE associate directly. TACE was pulled down by anti-FLAG antibody-conjugated beads when incubated with NRDc-FLAG (16% of the total input) (Fig. 5*A*). The coexistence of HB-EGF (soluble mature form) did not significantly affect the interaction of NRDc with TACE. Next, to determine whether NRDc is sufficient for TACE activation, we performed an *in vitro* peptide cleavage assay using the fluorescence-quenching peptide substrate corresponding to the cleavage site of HB-EGF. Although recombinant NRDc did not cleave the peptide, TACE did, as reported previously (14). Addition of NRDc to TACE significantly increased the amount of cleaved peptide in a dose-dependent manner (Fig. 5*B*). To identify the cleavage site, the cleaved product was analyzed by mass spectrometry. Analysis of the (TACE plus NRDc)-cleaved peptide showed an identical cleavage pattern as for the TACE-cleaved peptide, although the signal was much more intense in the TACE plus NRDc sample (Fig. 5*C*). These results confirm that NRDc is a potent activator of TACE in HB-EGF peptide cleavage and that the interaction with NRDc is sufficient for the activation.

Inhibition of NRDc Expression Results in Decreased Shedding of HB-EGF—To confirm that NRDc is essential for ectodomain shedding of HB-EGF, RNA-mediated interference was used to inhibit its expression. The effect of two distinct siRNA duplexes against NRDc and two control siRNAs on HB-EGF shedding was examined in COS-7 cells. Transfection of the siRNAs against NRDc resulted in a reduction of endogenous NRDc protein expression by 80.9 ± 3.1% (NRDc-1) and 80.4 ± 8.3% (NRDc-2), respectively, whereas the siRNAs did not affect the expression levels of TACE, HB-EGF, and GAPDH (Fig. 6, *A* and *B*). Constitutive HB-EGF shedding in siRNA-treated cells was significantly decreased (27.3 ± 4.0% by NRDc-1 ($p = 0.003$) and 22.3 ± 13.5% by NRDc-2 ($p = 0.02$)) compared with that in control siRNA (Control-1)-treated cells (Fig. 6*C*). PMA-induced HB-EGF shedding was also reduced to

a greater extent in those cells (34.0 ± 7.6% by NRDc-1 (p = 0.003) and 27.3 ± 11.3% by NRDc-2 (p = 0.006)). These results further establish that NRDc plays a critical role in both the constitutive and inducible ectodomain shedding of HB-EGF.

DISCUSSION

Our findings have identified NRDc, a metalloendopeptidase of the M16 family, as a potent activator of HB-EGF ectodomain shedding. The effect of NRDc appears not to be direct, but to be mediated by TACE because 1) an enzymatically inactive mutant of NRDc also enhanced the shedding, 2) NRDc and TACE cooperated to enhance the shedding in a cell-based assay, and 3) NRDc enhanced the catalytic activity of TACE in an *in vitro* peptide cleavage assay using a HB-EGF cleavage site peptide. We also demonstrated that NRDc and TACE form a complex in cells and direct interaction of the recombinant proteins. These results suggest that NRDc potentiates TACE activities via direct interaction. We examined TACE first because several lines of evidence have indicated that it is a specific sheddase for HB-EGF (14, 19, 34). Moreover, TACE is involved in ectodomain shedding of numerous membrane proteins and is recognized as the prototypical sheddase among ADAM proteins (1, 36). Of course, we cannot exclude the possibility that NRDc enhances the catalytic activities of other ADAM proteins or matrix metalloproteinases, which is an important issue to be resolved.

Phorbol esters (*e.g.* PMA) have been used as general activators of ectodomain shedding in many studies (1, 2, 36). However, the mechanism that underlies the activation of shedding was unclear. Here, we have demonstrated that NRDc forms a complex with TACE and that the process is potentiated by PMA, although PMA does not affect the total amounts of these proteins. Pulldown assays and *in vitro* peptide cleavage assays revealed that NRDc bound to the extracellular domain and potentiated the activity of TACE. These results indicate that the PMA-induced formation of a complex with NRDc at least partially explains how PMA activates TACE in HB-EGF shedding. However, the precise mechanism by which the formation of the complex is enhanced has not been clarified. NRDc is a cytosolic enzyme with no signal peptide; however, it is exported out of the cell by unknown mechanisms (27–29). The translocation of NRDc from the cytosol to the cell surface might nicely explain how the formation of a complex with TACE is enhanced by PMA without any significant change in the total expression level of the protein. Our staining data support this idea because PMA increased NRDc expression on plasma membranes, where NRDc and TACE mainly co-localized. Further study (for example, time-lapse observations of NRDc and TACE by confocal microscopy or a cell-surface biotinylation study) will be required to understand the regulation of NRDc translocation and the PMA-inducible interaction of NRDc with TACE.

Our findings indicate that NRDc is required for ectodomain shedding of HB-EGF because inhibition of its expression by RNA interference was accompanied by a reduction in constitutive and PMA-induced shedding. Several reasons for the relatively small effect of siRNA on the shedding (NRDc-1 siRNA, 27.3% for constitutive shedding and 34.0% for stimulated shedding) can be proposed. 1) The remnant of NRDc (20% of total expression) might be enough to enhance HB-EGF shedding. 2) There are unidentified proteins that have redundancy for NRDc in the shedding-enhancing effect. 3) Cell-surface NRDc might be less affected by gene knockdown because of the difference in stability between cell-surface and cytosolic NRDc. These possibilities are under investigation.

We identified NRDc as a protein that specifically binds HB-EGF (23) and demonstrated that the heparin-binding domain of HB-EGF is critically involved in the binding (29). Here, an *in vitro* peptide cleavage assay showed that NRDc enhanced the catalytic activity of TACE. The peptide used in the assay has only 8 amino acids corresponding to the juxtamembrane domain of HB-EGF. These results indicate that the effect of NRDc on the activity of TACE for ectodomain shedding of HB-EGF is not dependent on the capacity of NRDc to bind HB-EGF. In other words, the effect of NRDc might not be specific to HB-EGF, but might apply to a broader range of membrane substrates of TACE. Our pilot study suggested that NRDc enhances ectodomain shedding of multiple TACE substrates, including other EGFR ligands, tumor necrosis factor-α, and amyloid-β precursor protein.[3] The similar pattern of distribution of TACE and NRDc mRNAs found in most tissues and the especially high levels in heart, skeletal muscle, and testis (26, 32) support the idea that NRDc acts as a general activator of TACE in a physiological context. When NRDc-deficient animals become available, studies with them should show that NRDc is essential in the modulation of TACE activity and ectodomain shedding *in vivo*.

NRDc is a metalloendopeptidase that belongs to the M16 family. An enzymatically inactive NRDc mutant containing an altered active site retained the ability to enhance the catalytic activity of TACE and ectodomain shedding of HB-EGF. We have also demonstrated that the enzymatic activity of NRDc is not required for binding HB-EGF or the enhancement of cell migration (23). A metalloprotease activity-independent function of a M16 family member has been indicated for the *Saccharomyces cerevisiae AXL1* gene product, Axl1p, which is essential for the processing of propheromones and the selection of bud sites in yeast. The enzymatic activity is required for the former, but not the latter (38, 39). Although no substrates for NRDc *in vivo* have been identified, NRDc may act as a multifunctioning protein like Axl1p.

These findings imply that the activation of HB-EGF shedding can be blocked by inhibiting the interaction between NRDc and TACE. If true, NRDc could be an attractive therapeutic target for cancer and cardiovascular diseases because the EGFR signaling pathway is already an approved therapeutic target for cancer and because HB-EGF ectodomain shedding has been implicated in those diseases (8, 13, 40). Our findings have revealed a novel mechanism by which ectodomain shedding of HB-EGF is regulated. More studies on NRDc-TACE interactions will shed light on potential anti-shedding therapies.

[3] Y. Hiraoka, K. Yoshida, M. Ohno, K. Okawa, T. Kita, and E. Nishi, manuscript in preparation.

Acknowledgments—We thank N. Nishimoto for excellent technical assistance; K. Yoshino, M. Tanaka, S. Higashiyama, K. Matsumoto, and M. E. Milla for materials; and P. W. Park and R. A. Black for critically reading the manuscript.

REFERENCES

1. Arribas, J., and Borroto, A. (2002) *Chem. Rev.* **102,** 4627–4638
2. Blobel, C. P. (2005) *Nat. Rev. Mol. Cell Biol.* **6,** 32–43
3. Schlondorff, J., and Blobel, C. P. (1999) *J. Cell Sci.* **112,** 3603–3617
4. Kheradmand, F., and Werb, Z. (2002) *BioEssays* **24,** 8–12
5. Higashiyama, S., Abraham, J. A., Miller, J., Fiddes, J. C., and Klagsbrun, M. (1991) *Science* **251,** 936–939
6. Goishi, K., Higashiyama, S., Klagsbrun, M., Nakano, N., Umata, T., Ishikawa, M., Mekada, E., and Taniguchi, N. (1995) *Mol. Biol. Cell* **6,** 967–980
7. Iwamoto, R., and Mekada, E. (2000) *Cytokine Growth Factor Rev.* **11,** 335–344
8. Nishi, E., and Klagsbrun, M. (2004) *Growth Factors* **22,** 253–260
9. Suzuki, M., Raab, G., Moses, M. A., Fernandez, C. A., and Klagsbrun, M. (1997) *J. Biol. Chem.* **272,** 31730–31737
10. Yu, W. H., Woessner, J. F., Jr., McNeish, J. D., and Stamenkovic, I. (2002) *Genes Dev.* **16,** 307–323
11. Izumi, Y., Hirata, M., Hasuwa, H., Iwamoto, R., Umata, T., Miyado, K., Tamai, Y., Kurisaki, T., Sehara-Fujisawa, A., Ohno, S., and Mekada, E. (1998) *EMBO J.* **17,** 7260–7272
12. Yan, Y., Shirakabe, K., and Werb, Z. (2002) *J. Cell Biol.* **158,** 221–226
13. Asakura, M., Kitakaze, M., Takashima, S., Liao, Y., Ishikura, F., Yoshinaka, T., Ohmoto, H., Node, K., Yoshino, K., Ishiguro, H., Asanuma, H., Sanada, S., Matsumura, Y., Takeda, H., Beppu, S., Tada, M., Hori, M., and Higashiyama, S. (2002) *Nat. Med.* **8,** 35–40
14. Sunnarborg, S. W., Hinkle, C. L., Stevenson, M., Russell, W. E., Raska, C. S., Peschon, J. J., Castner, B. J., Gerhart, M. J., Paxton, R. J., Black, R. A., and Lee, D. C. (2002) *J. Biol. Chem.* **277,** 12838–12845
15. Dethlefsen, S. M., Raab, G., Moses, M. A., Adam, R. M., Klagsbrun, M., and Freeman, M. R. (1998) *J. Cell. Biochem.* **69,** 143–153
16. Hirata, M., Umata, T., Takahashi, T., Ohnuma, M., Miura, Y., Iwamoto, R., and Mekada, E. (2001) *Biochem. Biophys. Res. Commun.* **283,** 915–922
17. Prenzel, N., Zwick, E., Daub, H., Leserer, M., Abraham, R., Wallasch, C., and Ullrich, A. (1999) *Nature* **402,** 884–888
18. Yamazaki, S., Iwamoto, R., Saeki, K., Asakura, M., Takashima, S., Yamazaki, A., Kimura, R., Mizushima, H., Moribe, H., Higashiyama, S., Endoh, M., Kaneda, Y., Takagi, S., Itami, S., Takeda, N., Yamada, G., and Mekada, E. (2003) *J. Cell Biol.* **163,** 469–475
19. Jackson, L. F., Qiu, T. H., Sunnarborg, S. W., Chang, A., Zhang, C., Patterson, C., and Lee, D. C. (2003) *EMBO J.* **22,** 2704–2716
20. Iwamoto, R., Yamazaki, S., Asakura, M., Takashima, S., Hasuwa, H., Miyado, K., Adachi, S., Kitakaze, M., Hashimoto, K., Raab, G., Nanba, D., Higashiyama, S., Hori, M., Klagsbrun, M., and Mekada, E. (2003) *Proc. Natl. Acad. Sci. U. S. A.* **100,** 3221–3226
21. Chen, B., Bronson, R. T., Klaman, L. D., Hampton, T. G., Wang, J. F., Green, P. J., Magnuson, T., Douglas, P. S., Morgan, J. P., and Neel, B. G. (2000) *Nat. Genet.* **24,** 296–299
22. Dong, J., Opresko, L. K., Dempsey, P. J., Lauffenburger, D. A., Coffey, R. J., and Wiley, H. S. (1999) *Proc. Natl. Acad. Sci. U. S. A.* **96,** 6235–6240
23. Nishi, E., Prat, A., Hospital, V., Elenius, K., and Klagsbrun, M. (2001) *EMBO J.* **20,** 3342–3350
24. Chesneau, V., Pierotti, A. R., Barre, N., Creminon, C., Tougard, C., and Cohen, P. (1994) *J. Biol. Chem.* **269,** 2056–2061
25. Pierotti, A. R., Prat, A., Chesneau, V., Gaudoux, F., Leseney, A. M., Foulon, T., and Cohen, P. (1994) *Proc. Natl. Acad. Sci. U. S. A.* **91,** 6078–6082
26. Fumagalli, P., Accarino, M., Egeo, A., Scartezzini, P., Rappazzo, G., Pizzuti, A., Avvantaggiato, V., Simeone, A., Arrigo, G., Zuffardi, O., Ottolenghi, S., and Taramelli, R. (1998) *Genomics* **47,** 238–245
27. Chesneau, V., Prat, A., Segretain, D., Hospital, V., Dupaix, A., Foulon, T., Jegou, B., and Cohen, P. (1996) *J. Cell Sci.* **109,** 2737–2745
28. Hospital, V., Chesneau, V., Balogh, A., Joulie, C., Seidah, N. G., Cohen, P., and Prat, A. (2000) *Biochem. J.* **349,** 587–597
29. Hospital, V., Nishi, E., Klagsbrun, M., Cohen, P., Seidah, N. G., and Prat, A. (2002) *Biochem. J.* **367,** 229–238
30. Gechtman, Z., Alonso, J. L., Raab, G., Ingber, D. E., and Klagsbrun, M. (1999) *J. Biol. Chem.* **274,** 28828–28835
31. Tokumaru, S., Higashiyama, S., Endo, T., Nakagawa, T., Miyagawa, J. I., Yamamori, K., Hanakawa, Y., Ohmoto, H., Yoshino, K., Shirakata, Y., Matsuzawa, Y., Hashimoto, K., and Taniguchi, N. (2000) *J. Cell Biol.* **151,** 209–220
32. Black, R. A., Rauch, C. T., Kozlosky, C. J., Peschon, J. J., Slack, J. L., Wolfson, M. F., Castner, B. J., Stocking, K. L., Reddy, P., Srinivasan, S., Nelson, N., Boiani, N., Schooley, K. A., Gerhart, M., Davis, R., Fitzner, J. N., Johnson, R. S., Paxton, R. J., March, C. J., and Cerretti, D. P. (1997) *Nature* **385,** 729–733
33. Moss, M. L., Jin, S. L., Milla, M. E., Bickett, D. M., Burkhart, W., Carter, H. L., Chen, W. J., Clay, W. C., Didsbury, J. R., Hassler, D., Hoffman, C. R., Kost, T. A., Lambert, M. H., Leesnitzer, M. A., McCauley, P., McGeehan, G., Mitchell, J., Moyer, M., Pahel, G., Rocque, W., Overton, L. K., Schoenen, F., Seaton, T., Su, J. L., Warner. J., Willard, D., and Becherer, J. D. (1997) *Nature* **385,** 733–736
34. Sahin, U., Weskamp, G., Kelly, K., Zhou, H. M., Higashiyama, S., Peschon, J., Hartmann, D., Saftig, P., and Blobel, C. P. (2004) *J. Cell Biol.* **164,** 769–779
35. Higashiyama, S., Lau, K., Besner, G. E., Abraham, J. A., and Klagsbrun, M. (1992) *J. Biol. Chem.* **267,** 6205–6212
36. Black, R. A., Doedens, J. R., Mahimkar, R., Johnson, R., Guo, L., Wallace, A., Virca, D., Eisenman, J., Slack, J., Castner, B., Sunnarborg, S. W., Lee, D. C., Cowling, R., Jin, G., Charrier, K., Peschon, J. J., and Paxton, R. (2003) *Biochem. Soc. Symp.* **70,** 39–52
37. Doedens, J. R., and Black, R. A. (2000) *J. Biol. Chem.* **275,** 14598–14607
38. Fujita, A., Oka, C., Arikawa, Y., Katagai, T., Tonouchi, A., Kuhara, S., and Misumi, Y. (1994) *Nature* **372,** 567–570
39. Adames, N., Blundell, K., Ashby, M. N., and Boone, C. (1995) *Science* **270,** 464–467
40. Tanaka, Y., Miyamoto, S., Suzuki, S. O., Oki, E., Yagi, H., Sonoda, K., Yamazaki, A., Mizushima, H., Maehara, Y., Mekada, E., and Nakano, H. (2005) *Clin. Cancer Res.* **11,** 4783–4792

Real-Time 2-Photon Imaging of Mitochondrial Function in Perfused Rat Hearts Subjected to Ischemia/Reperfusion

Madoka Matsumoto-Ida, MD; Masaharu Akao, MD, PhD; Toshihiro Takeda, MD; Masashi Kato, MD; Toru Kita, MD, PhD

Background—Mitochondria play pivotal roles in cell death; the loss of mitochondrial membrane potential ($\Delta\Psi_m$) is the earliest event that commits the cell to death. Here, we report novel real-time imaging of $\Delta\Psi_m$ in individual cardiomyocytes within perfused rat hearts using 2-photon laser-scanning microscopy, which has unique advantages over conventional confocal microscopy: greater tissue penetration and lower tissue toxicity.

Methods and Results—The Langendorff-perfused rat heart was loaded with a fluorescent indicator of $\Delta\Psi_m$, tetramethylrhodamine ethyl ester. Tetramethylrhodamine ethyl ester was excited with an 810-nm line of a Ti:sapphire laser, and its fluorescence in the heart cells was successfully visualized up to ≈50 μm from the epicardial surface. Taking advantage of this system, we monitored the spatiotemporal changes of $\Delta\Psi_m$ in response to ischemia/reperfusion at the subcellular level. No-flow ischemia caused progressive $\Delta\Psi_m$ loss and a more prominent $\Delta\Psi_m$ loss on reperfusion. During ischemia/reperfusion, cells maintained a constant $\Delta\Psi_m$ for the cell-to-cell specific period of latency, followed by a rapid, complete, and irreversible $\Delta\Psi_m$ loss, and this process did not affect the neighboring cells. Within a cell, $\Delta\Psi_m$ loss was initiated in a particular area of mitochondria and rapidly propagated along the longitudinal axis. These spatiotemporal changes in $\Delta\Psi_m$ resulted in marked cellular and subcellular heterogeneity of mitochondrial function. Ischemic preconditioning reduced the number of cells undergoing $\Delta\Psi_m$ loss, whereas cyclosporin A partially inhibited $\Delta\Psi_m$ loss in each cell.

Conclusions—Investigation of cellular responses in the natural environment will increase knowledge of ischemia/reperfusion injury and provide deeper insights into antiischemia/reperfusion therapy that targets mitochondria. **(*Circulation*. 2006;114:1497-1503.)**

Key Words: imaging ■ ischemia ■ reperfusion ■ mitochondria

Mitochondria are crucial regulators of life and death in a variety of cells[1,2] and play pivotal roles in cardiomyocyte death in response to myocardial ischemia/reperfusion.[3,4] The loss of mitochondrial membrane potential ($\Delta\Psi_m$) is the earliest event that commits the cell to death, and this process is potentially a prime target for therapeutic interventions.[5,6] We and other investigators have studied the spatiotemporal changes in $\Delta\Psi_m$ using confocal imaging of isolated cardiomyocytes in vitro that were exposed to a variety of stresses.[7–12] Investigation of such time-dependent changes in mitochondrial function within single cardiomyocytes of an intact living heart would have tremendous advantages over the in vitro models, because the heart is working as a syncytium in which individual cardiomyocytes are anatomically and functionally connected. Moreover, the pathological stimulus (ischemia/reperfusion) applied to the intact heart model is more clinically relevant to ischemic heart disease in humans than those used in the in vitro models, such as oxidant stress,[7–9] metabolic inhibition,[10] hypoxia,[11] glucose deprivation,[12] or other insults. The visualization of mitochondrial function in the living heart has been a technically difficult task for conventional confocal imaging, however, because the heart tissue is highly light-scattering, and mitochondria are quite susceptible to photodamage.

Editorial p 1452
Clinical Perspective p 1503

Two-photon laser-scanning microscopy (TPLSM) has unique advantages over conventional single-photon confocal microscopy.[13,14] First, the penetration depth of the excitation beam is increased. Second, because no out-of-focus fluorescence is generated, no pinhole is necessary during image acquisition, which results in increased fluorescence collection efficiency. Third, 2-photon excitation markedly reduces overall photobleaching and photodamage, which results in extended viability of biological specimens during long-term imaging. These properties are particularly advantageous in monitoring mitochondrial function in the living heart.

Taking advantage of these properties of TPLSM, we, for the first time, successfully visualized $\Delta\Psi_m$ in ex vivo heart

Received March 22, 2006; revision received June 26, 2006; accepted July 14, 2006.
From the Department of Cardiovascular Medicine, Kyoto University Graduate School of Medicine, Kyoto, Japan.
The online-only Data Supplement is available with this article at http://circ.ahajournals.org/cgi/content/full/CIRCULATIONAHA.106.628834/DC1.
Correspondence to Masaharu Akao, MD, PhD, Department of Cardiovascular Medicine, Kyoto University Graduate School of Medicine, 54 Kawahara-cho, Shogoin, Sakyo-ku, Kyoto 606-8507, Japan. E-mail akao@kuhp.kyoto-u.ac.jp

Circulation **is available at http://www.circulationaha.org** **DOI: 10.1161/CIRCULATIONAHA.106.628834**

specimens and monitored the progressive changes of $\Delta\Psi_m$ in response to ischemia/reperfusion. Direct imaging of these spatial and temporal changes in mitochondrial function would revolutionize our understanding of ischemia/reperfusion injury and provide deeper insights into the establishment of a novel cardioprotective therapy that targets mitochondria.

Methods

All procedures were performed in accordance with the Kyoto University animal experimentation committee, which conforms to the "Guide for the Care and Use of Laboratory Animals" published by the US National Institutes of Health.

Langendorff-Perfused Rat Heart

Adult Sprague-Dawley rats (weighing 250 to ≈300 g, all females; Shimizu Laboratory Supplies, Kyoto, Japan) were used for all studies. The heart was excised, the ascending aorta was cannulated with a customized needle, and hearts were perfused in the Langendorff mode. Perfusion was performed at a constant mean perfusion pressure with oxygenated (95% O_2) Tyrode's solution containing (in mmol/L) 134 NaCl, 4 KCl, 1.2 $MgSO_4$, 1.2 NaH_2PO_4, 10 HEPES, 11 D-glucose, and 2 $CaCl_2$ (pH 7.4, adjusted with 1 mol/L NaOH). After loading of fluorescent indicators as indicated below, the heart was perfused further by a solution containing 10 mmol/L 2,3-butanedione monoxime (BDM) for 15 minutes to eliminate contraction-induced movement of the heart and was placed in a circular glass-bottomed dish (35-mm diameter) for 2-photon imaging. To optimize the focal plane, the heart was gently pressed against the coverslip (170-μm thickness) at the bottom of the chamber.

Loading of Fluorescent Dyes

After an initial perfusion period of ≈10 minutes, the buffer was switched to Tyrode's solution containing 100 nmol/L tetramethylrhodamine ethyl ester (TMRE; Molecular Probes; Eugene, Ore), which is an indicator of $\Delta\Psi_m$, and this was followed by a 20-minute washout with dye-free solution.

Cytolysis was monitored with 20 μmol/L 2′,7′-bis-(2-carboxyethyl)-5-(and-6)-carboxyfluorescein, acetoxymethyl ester (BCECF-AM; Molecular Probes). After a 30-minute loading period, the heart was perfused with dye-free Tyrode's solution for 20 minutes to allow for deesterification of the dyes by endogenous esterases. In this case, the heart was further loaded with TMRE, followed by washout. The detection of cell death was also performed by staining with propidium iodide (PI; Molecular Probes). In this experiment, the heart was preloaded with TMRE and BCECF-AM and subjected to 30 minutes of ischemia followed by 30 minutes of reperfusion. At the end of the experimental period, the heart was further loaded with PI by perfusing it with Tyrode's solution containing PI 1.5 mmol/L for 20 minutes.

Ischemia/Reperfusion Protocol

The perfusate was equilibrated with 95% O_2 (pH 7.4). The temperature was maintained at 37°C with a solution heater and a platform heater (Warner Instruments; Hamden, Conn) installed on the microscope stage. After a stabilization period (≈10 minutes), the hearts were subjected to either ischemia (60 minutes; myocardial ischemia [MI]) or ischemia/reperfusion (30 minutes/30 minutes; MI/reperfusion [MI/R]). Ischemia was achieved by clamping the perfusion line. Reperfusion was achieved by releasing the clamp. In the cyclosporin A (CsA)–treated group, the hearts were treated with CsA 0.2 or 1.0 μmol/L dissolved in the perfusate for 30 minutes immediately before BDM treatment and MI/R. In the ischemic preconditioning (IPC) group, 3 cycles of 5 minutes of ischemia and 5 minutes of reperfusion were followed by BDM treatment and MI/R.

Two-Photon Laser-Scanning Microscopy

Images were recorded with a Zeiss LSM510 laser scanning microscope (Carl Zeiss MicroImaging GmbH, Jena, Germany) modified for TPLSM. Illumination for 2-photon excitation was provided by a mode-locked Ti:sapphire laser (Spectra-Physics; Irvine, Calif); the excitation wavelength was 810 nm. Hearts were imaged through a Zeiss 63× 1.40 numerical aperture oil-immersion objective with a working distance of 180 μm (Carl Zeiss Microimaging, Inc). Emitted light was collected by 2 photomultiplier tubes fitted with band-pass filters for 500 to 550 nm (for BCECF-AM) and 565 to 615 nm (for TMRE and PI), respectively. For full-frame-mode analyses (512×512 pixels), hearts were scanned on horizontal (x, y) planes, and the resulting images were digitized at an 8-bit resolution and stored directly on a hard disk. The images are representative ones from at least 3 independent experiments, and we have confirmed the reproducibility of the responses.

Image Analysis

Postacquisition analysis was performed with an image-analysis software program (ImageJ, National Institutes of Health; available at http://rsb.info.nih.gov/ij/). From the image sequences, we quantitatively assessed the kinetics of $\Delta\Psi_m$ loss in individual cells. Regions of interest were drawn over a part of an individual cell, and fluorescence signals within these regions were collected over time. $\Delta\Psi_m$ was monitored by mean TMRE brightness within the regions. Three-dimensional image processing was performed with a software program (Imaris; Bitplane Inc; St Paul, Minn).

Statistical Analysis

Quantitative data are presented as mean±SEM. Comparisons were performed with either the unpaired Student t test or 1-way ANOVA with Bonferroni procedure as the post hoc test. A level of $P<0.05$ was accepted as statistically significant.

The authors had full access to the data and take full responsibility for its integrity. All authors have read and agree to the manuscript as written.

Results

We visualized mitochondria in the Langendorff-perfused rat heart loaded with TMRE, a fluorescent indicator of $\Delta\Psi_m$ (Figure 1). Tightly focused images of TMRE fluorescence could be obtained at various depths up to ≈50 μm (≈3 to 4 layers of myocardial cells) below the epicardial surface of the heart (Figure 1B; online-only Data Supplement, Movie I). The temporal resolution was sufficient to observe each single mitochondrion (Figure 1C). The image clearly demonstrates that cardiomyocytes have considerable numbers of mitochondria aligned in an orderly fashion along the myofilaments. Three-dimensional image reconstruction was made possible by stacking the optical slices with 3-dimensional processing software (Figure 1D; online Data Supplement, Movie II).

Using this imaging system, we monitored $\Delta\Psi_m$ changes in perfused hearts subjected to ischemia/reperfusion. Time-lapse images were taken every 5 minutes (Figure 2A). Control perfusion with oxygenated Tyrode's solution maintained $\Delta\Psi_m$ for >60 minutes (Figure 2A, control). No-flow MI (60 minutes of ischemia) caused progressive $\Delta\Psi_m$ loss (Figure 2A, MI; online Data Supplement, Movie III). In the MI/R group (30 minutes of ischemia followed by 30 minutes of reperfusion), there was progressive $\Delta\Psi_m$ loss during the ischemic period and a more prominent $\Delta\Psi_m$ loss on reperfusion (Figure 2A, MI/R; online Data Supplement, Movie IV). The $\Delta\Psi_m$ loss was sporadically initiated over the observation area (arrows in Figure 2A, MI and MI/R). Figure 2B shows the time courses of fluorescence obtained from representative cells. In both the MI and MI/R groups, ischemia/reperfusion did not immediately result in $\Delta\Psi_m$ loss; instead, there was a